Science of the Total Environment 666 (2019) 928–943

Contents lists available at ScienceDirect

Science of the Total Environment

journal homepage: www.elsevier.com/locate/scitotenv

Modelling permafrost thickness in Great Britain over glacial cycles

Johanna M. Scheidegger [a,*], Christopher R. Jackson [a], Fiona M. McEvoy [a], Simon Norris [b]

[a] British Geological Survey, Environmental Science Centre, Keyworth, Nottingham NG12 5GG, UK
[b] Radioactive Waste Management Limited, Curie Avenue, Harwell, Didcot OX11 0RH, UK

HIGHLIGHTS

- Permafrost development considered within context of geological disposal of waste
- Two contrasting geological settings within Great Britain
- Coupled permafrost and groundwater flow modelling to estimate permafrost thickness
- Relative importance of physical properties and thermal boundary conditions assessed.
- Uncertainty in surface temperatures is largest influence on permafrost thickness.

GRAPHICAL ABSTRACT

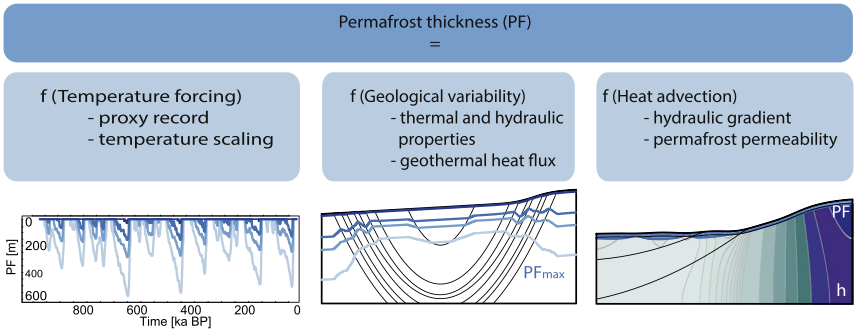

ARTICLE INFO

Article history:
Received 2 August 2018
Received in revised form 4 February 2019
Accepted 9 February 2019
Available online 15 February 2019

Editor: Ralf Ludwig

Keywords:
Permafrost
Glacial-interglacial time-scales
Geological disposal
Numerical modelling

ABSTRACT

Like other countries, the UK has opted for deep geological disposal for the long-term, safe management of higher-activity radioactive waste. However, a site and a geological environment have yet to be identified to host a geological disposal facility. In considering its long-term safety functionality, it is necessary to consider natural processes, such as permafrost development, that have the potential to alter the geological environment over the time-scale of glacial-interglacial cycles. We applied a numerical model to simulate the impact of long-term climatic variability on groundwater flow and permafrost dynamics in two contrasting geological settings in Great Britain: (i) higher strength rocks (HSR) overlain by higher permeability sandstones with a high topographic gradient (GS1); (ii) a mixed sedimentary sequence of high and low permeability rocks resting on igneous HSR with a very low topographic gradient (GS2). We evaluated the sensitivity of simulated permafrost thickness to a variety of climatic and subsurface conditions. Uncertainty in the scaling of the surface temperature time-series, 10–25 °C below present day temperature, has the largest impact on maximum permafrost thickness, PF_{max}, compared to other variables. However, considering plausible parameter ranges for UK settings, PF_{max} is up to twice as sensitive to changes in thermal conductivity and geothermal heat flux than to changes in porosity. Heat advection only affects modelled PF_{max} for high hydraulic conductivity rocks and if permafrost is considered to be relatively permeable. Whilst local differences in permafrost thickness of tens of meters, caused by variations in heat advection, are of minor importance over glacial-interglacial cycles, heat advection can be important in the development of taliks and the maintenance of a more active groundwater flow system. We conclude that it is likely to be important to simulate the effect of heat advection on coupled permafrost and groundwater flow systems in settings containing higher permeability lithological sequences.

* Corresponding author.
E-mail address: johsch@bgs.ac.uk (J.M. Scheidegger).

https://doi.org/10.1016/j.scitotenv.2019.02.152

1. Introduction

The disposal of radioactive waste represents a significant challenge for countries with developed or past nuclear industries. Most countries, including the UK, have opted for deep geological disposal for the long-term, safe and secure management of higher activity radioactive waste (DECC, 2014). The deep geological disposal of radioactive waste differs from other sub-surface exploitation in that it requires significant assessment, to understand the impact of potential fugitive radionuclides, for up to 1 million years into the future; such a timescale reflects the length of time for the radioactivity of typical waste materials to be significantly reduced by natural decay (McEvoy et al., 2016).

Deep geological disposal involves the emplacement of wastes in an engineered facility at depths of between 200 m and 1000 m below the land surface, making use of the surrounding geological environment as one of the many barriers to ensure that no harmful quantities of radioactivity ever reach the surface environment (NDA, 2010). The geological environment provides two functions: to contain the radionuclides and to isolate the disposed waste from the surface environment. The geological environment should be relatively stable to ensure the waste is isolated from the biosphere for the long-term and its behaviour adequately predictable to enable scientifically sound evaluations of the long-term radiological safety of a disposal facility (IAEA, 2011).

In the UK, a site and a geological environment has yet to be identified to host a disposal facility. In 2014, the UK embarked on a new programme to identify a site (DECC, 2014) commencing with a national campaign to collate national-scale geological information for a range of geological attributes of relevance to assessing long-term safety (RWM, 2016).

In considering the long-term safety functionality of a geological disposal facility (GDF), it is necessary to take account of natural processes that have the potential to alter the geological environment over the time-scale of glacial-interglacial cycles. Predicting climate system evolution over glacial-interglacial time-scales is a significant challenge and highly uncertain (McEvoy et al., 2016), and relies on estimating the extremes within which climate and climate-related processes may vary with reasonable confidence (Nasir et al., 2013). Longer-term climate projections forecast that the Northern Hemisphere will experience further cycling between glacial and interglacial periods over the next 100,000 to 1 million years (Näslund and Brandefelt, 2014). A disposal facility in the UK is therefore likely to experience glaciation and/or permafrost conditions several times over its lifetime and hence, predictions of the duration, thickness and extent of future ice cover are important for assessing the post-closure safety of a UK GDF (McEvoy et al., 2016). Permafrost is defined as ground with temperature below 0 °C, regardless whether its water is in liquid or frozen state (Woo, 2012). Permafrost forms when the mean annual ground surface temperature is below 0 °C (Williams and Smith, 1989), which is likely to occur during glacial cycles when the location is not covered by an ice sheet. Therefore, along with the consideration of other impacts, an environmental safety case requires the assessment of the effect of permafrost on a potential geological environment including the depth of permafrost (McEvoy et al., 2016)

Possible effects of permafrost on a GDF can either be direct, when permafrost reaches the depth of a GDF, or via associated impacts, when the permafrost depth does not reach the GDF itself, but alters the sub-permafrost environment. Direct effects include phase change of available pore water to pore ice, which results in pressure changes induced by the volume change from the phase change of water to ice. This can result in mechanical effects of freezing and thawing on rock stability, which can reduce the performance of the engineered components of a GDF, such as clay (McEwen and de Marsily, 1991). Both within and underneath the permafrost, changes in the chemical composition of groundwater due to freeze-out of solutes can result in the formation of cryopegs: supercooled unfrozen zones that are perennially below 0 °C and are perennially unfrozen due to their elevated solute concentration (Woo, 2012). Alteration of groundwater chemistry, such as increased salinity, has the potential to impact the performance of any bentonite in the engineered barrier of a GDF or in sealed access shafts (McEwen and de Marsily, 1991). Beneath permafrost, groundwater flow is affected by a reduction of recharge and discharge, and the focussing of groundwater flow through taliks, unfrozen zones within the permafrost. Taliks may occur under surface water bodies, and around any high permeability fracture zones (Ruskeemiemi et al., 2002).

To estimate such potential impacts, a few studies have modelled groundwater and permafrost dynamics over glacial time-scales. These have principally been related to GDF assessments undertaken by relevant institutions in Sweden (SKB), Finland (POSIVA), France (Andra), Canada (NWMO), Belgium (SCK CEN) and Switzerland (NAGRA). Geological environments considered for coupled groundwater-permafrost modelling with respect of GDFs have included: fractured crystalline rock of the Fennoscandian Shield (Hartikainen et al., 2010; Vidstrand et al., 2014; Sterckx et al., 2018); the Canadian Shield (Lemieux et al., 2008a; Chan and Stanchell, 2009); sedimentary basins such as the Michigan Basin (Normani and Sykes, 2012; Nasir et al., 2013); a generic intercratonic basin at the southern limit of the Laurentide Ice Sheet (Bense and Person, 2008); and the Paris Basin (Holmén et al., 2011; Grenier et al., 2013).

The results of the studies in Sweden, France, and Canada cannot be translated directly to a setting in Great Britain, since both geology and climatic history are different. The geographical situation in Great Britain on the north-western margin of Europe, combined with its complex tectonic history giving rise to highly varied geology and topography, mean that it has distinctive factors that are likely to influence the effects of future climatic-driven processes on a GDF when compared to assessments undertaken by other radioactive waste disposal programs in northern latitudes such as Sweden and Finland (e.g. SKB, 2011; Posiva, 2012; SKB, 2014). The mid-latitude position of Great Britain has proven particularly sensitive to past global-scale climatic changes with marked variations in prevailing climate over comparatively short periods of geological time (tens of thousands of years; (e.g. Rose, 2009; Candy and Lee, 2011) as a result of its position relative to southward moving cold polar air masses (Polar Front), and low latitude warm ocean currents (North Atlantic Current) (McEvoy et al., 2016). Lower latitude, geologically variable but stable intraplate locations such as in Great Britain pose different challenges and questions than that of tectonically active and/or recently deglaciated regions of the Northern Hemisphere.

It is only relatively recently that variations in permafrost thickness over glacial cycles have been modelled for settings within the UK. Busby et al. (2015, 2016) investigated the potential depth of permafrost using a 1D heat conduction model to simulate the 0 °C isotherm as a proxy for permafrost depth. These studies considered both geological variability, by applying the models to ten different locations across Great Britain, and climate variability, by using different surface temperatures scenarios, which included the thermal effects of an ice sheet. The thermal modelling suggested the depth of the 0 °C isotherm to be highly variable, depending on the geographical location and geological environment. The geographical location defines the local temperature and ice sheet history, and the geological environment defines the thermal properties that determine how fast, and to which depth, a temperature signal propagates into the subsurface.

Whilst Busby et al. (2015, 2016) investigated the influence of surface temperature histories and thermo-hydrogeological properties on modelled permafrost thickness by considering a number of different localities across Great Britain, they did not consider how groundwater flow and heat advection, or the phase change of water to ice, and associated latent heat of freezing and thawing, could affect predicted values. A question remains as to which of the following factors controlling permafrost thickness has the most influence on predicted values: surface temperature estimates, thermal and hydraulic properties of the subsurface, or heat advection and latent heat of freezing and thawing? This is of relevance to assessments both within the UK and elsewhere.

To simulate the effect of heat advection on permafrost dynamics, coupled models are required that incorporate the process of the variation in the hydraulic conductivity of the domain as permafrost forms and thaws i.e. as the ice saturation in pore space changes. Several experimental or theoretical relationships describing the change of hydraulic conductivity as a function of ice saturation or temperature over the freezing interval can be found in the literature for sand, silt, and clay (e.g. Burt and Williams, 1976; Kleinberg and Griffin, 2005; Watanabe and Flury, 2008; Azmatch et al., 2012). Furthermore, the decrease in relative hydraulic conductivity with ice saturation has been found to be different for different lithologies, with relative hydraulic conductivity decreasing by between three and eight orders of magnitude (Burt and Williams, 1976; Kleinberg and Griffin, 2005). Consequently, the parameterisation of this relationship in models is uncertain. With regard to thermo-hydrogeological properties of the subsurface, the identification of a potential host rock for a GDF may target lithologies with particular characteristics e.g. low hydraulic conductivity. However, considering the geological complexity of the UK, it is possible that the potential host rock could be located within a complex sequence of lithologies (RWM, 2016), the thermal and hydraulic properties of which span a broad range of values (Rollin, 1987; Busby et al., 2011).

There is large uncertainty in making future projections of surface temperature. Because of this, most previous studies that have simulated permafrost thickness in relation to a GDF assessment have applied a range of temperature scenarios derived by scaling past climate proxies (Hartikainen et al., 2010; Holmén et al., 2011; Nasir et al., 2013; Busby et al., 2016).

The objective of this work was to evaluate to which factors permafrost thickness is most sensitive to over glacial time-scales in the UK, including uncertainties in surface temperatures, thermo-hydrogeological properties, or changes in hydraulic conductivity as permafrost forms.

To investigate this, we developed coupled groundwater flow and heat transport models, incorporating heat conduction, advection, and water-ice phase change with associated latent heat effects for two contrasting geological settings within Great Britain over future glacial-interglacial cycles. These models were forced with a range of possible surface temperature boundary conditions and model parameterisations to investigate the effect of climate, geological variability, and heat advection, on permafrost thickness. In relation to the influence of heat advection, we specifically investigated the effect of the parameterisation of the ice content-hydraulic conductivity relationship on simulated maximum permafrost thickness. After considering when the application of 1D models, which do not represent groundwater flow and heat advection, is acceptable, we explored the sensitivity of permafrost thickness to thermo-hydrogeological properties using a much larger ensemble of 1D model simulations. The two geological setting we modelled were not considered to have a particular position within the British mainland, and therefore, were not directly associated with any history of ice sheet coverage. Partly because of this, and partly because it was beyond the scope of this study, we therefore, did not consider the influence of ice sheet coverage on the groundwater flow and permafrost dynamics. Rather we adopted the approach of assessing the sensitivity of the modelled system to imposed surface temperature time-series. The implications of not including the effect of ice sheets, is discussed in Section 4.5.3.

The paper is structured as follows. In Section 2, Methods, we describe the rationale for the selection of the two geological settings, and their structure, the derivation surface temperature scenarios over 1 million years, and the modelling methodology. In Section 3 we present the results of the modelling, detailing differences in permafrost thickness due to different surface temperature scenarios, physical thermo-hydrogeological properties and the influence of heat advection. The results are discussed in Section 4 within the context of a GDF, and conclusion drawn in Section 5.

2. Methods

2.1. Geological settings

The UK has a diverse geology, including many settings that may be suitable hosts for a GDF. Potentially suitable rock types are grouped into three broad categories: higher strength rocks (HSR); lower strength sedimentary rocks (LSSR); and evaporitic rocks (RWM, 2016). Higher strength rocks may be igneous, metamorphic or older sedimentary rocks, have a low matrix porosity and low permeability, with the majority of any groundwater movement confined to fractures within the rock mass. Lower strength sedimentary rocks are typically fine-grained, with a high content of clay minerals that provides their low permeability, and are mechanically weak so that open fractures cannot be sustained. They are typically interlayered with other sedimentary rock types.

In representing this variability of rock types when planning site investigations, developing disposal concepts and designs, and developing safety cases ahead of identifying a possible site, six illustrative geological environments have been conceptualised. These incorporate both higher strength rocks and lower strength sedimentary rocks, that collectively cover many of the geological and hydrogeological characteristics that are relevant to the majority of England, Wales and Northern Ireland (RWM, 2016). The development of these conceptual geological environments describes, at a high level, some of the geological and hydrogeological characteristics and data that need to be considered for planning and research purposes. These conceptual geological environments are generic, and not based on a specific location.

For this study, we selected two of these six geological environments that have clearly contrasting dominant host rock types, contrasting topography, proximity to the coast and structure. The two contrasting geological settings represent two end-members of different geological environments, a higher strength rock covered by higher strength sedimentary cover with a high topographic gradient and a sequence of higher and lower strength rock sedimentary rock overlying higher strength granitic and igneous rock with a low topographic gradient. These two geological settings enable us to understand the relative importance of hydrogeological and thermal properties, and advective heat flow on maximum permafrost depth. The two environments are represented by two-dimensional cross-sections, or vertical 'slices', both of which have been extended to include an upstream water divide. Hereafter, we refer to the two selected environments as geological setting 1 (GS1) and geological setting 2 (GS2).

GS1 (Fig. 1a) describes an environment comprising higher strength rocks as the host-rock, extending to the surface in areas of high relief and onlapped by a sequence of high permeability sandstones that thicken towards the basin centre. There are no lower permeability sedimentary rocks within the sedimentary sequence that could provide significant barriers of groundwater flow. Where it outcrops, the higher strength rocks are weathered to some degree. In this setting, recharge can occur directly to the higher strength rocks at outcrop or to the overlying sandstones. GS2 (Fig. 1b) describes a synclinal basin structure composed of a mixed sedimentary sequence of permeable (sandstones, limestones and Chalk) and lower permeability rocks (mudstones, siltstones, shales, and clay) resting on higher strength rocks. In this setting, both the higher strength rocks (units 8 and 9) and the lower permeability rocks (units 5 and 6) have the potential to act as a host-rock. The environment has a very low topographic relief and is hundreds of kilometers from the nearest areas of significant topography. Driving head gradients are therefore low. The presence of a lower permeability clay formation (unit 3) between the potential host rocks and the ground surface has the potential to isolate the surface environment and the recharge that occurs there. However, outcropping higher permeability formations (units 2 and 4, limestone; unit 7, sandstone) may carry significant flow to depth.

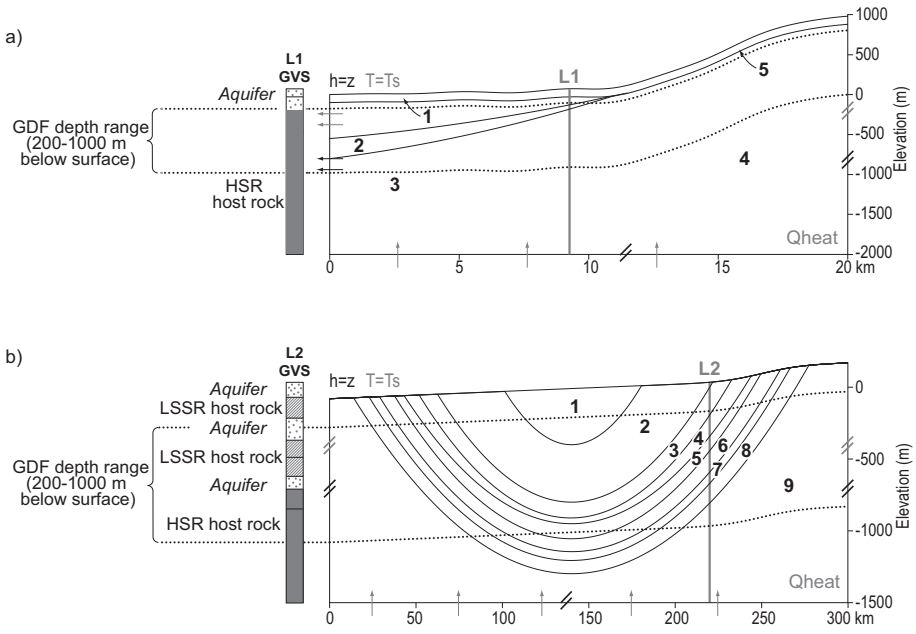

Fig. 1. Model set-up and boundary conditions for (a) GS1 and (b) GS2. The lithological units for GS1 are: (1) weathered sandstone; (2) upper sandstone; (3) lower sandstone; (4) quartzite/meta-lava; (5) weathered quartzite/meta-lava. For GS2 the lithological units are (1) chalk; (2) limestone; (3) clay; (4) limestone; (5) mudstones and shales; (6) mudstones and siltstones; (7) sandstone; (8) granitic rock; (9) basic igneous rock. The boundary conditions in grey correspond to head or flow, and those in black to temperature or heat flux. The generalised vertical sections (GVS) L1 and L2 are vertical profiles at each horizontal location.
After Towler et al. (2008), reproduced with permission from NDA.

We select one location along the cross-section of each setting (L1 in GS1; L2 in GS2) which we use to present time-series of the simulated permafrost thickness. L1 and L2 were chosen so that the depth of the host rock lies within the GDF depth range of 200–1000 m, and the geological sequence above would fit with the geological environments described. At L1, the potential host rock (higher strength rocks) extends from 1000 to 330 m below surface, whilst at L2, two potential host rocks exist: higher strength rocks between 1000 and 700 m and lower strength sedimentary rocks between 620 and 370 m below surface.

2.2. Temperature setting

2.2.1. Surface temperature history

The climate has oscillated between glacial and interglacial conditions in the past, as evidenced by paleo-climatic proxies such as deep ocean sediment records, lake sediments, or ice cores (e.g. Lisiecki and Raymo, 2005). Even with the consideration of anthropogenic climate change, longer-term projections of the northern hemisphere climate indicate a continuation of glacial-interglacial cycles (Fischer et al., 2015).

Such proxies have been used to estimate past temperatures in the UK. For example, mean annual temperatures during the Last Glacial Maximum (LGM) were estimated near London, southern England of −13 °C, or 24 °C below modern temperature, based on the occurrence of temperature-sensitive taxa in the fossil record (Atkinson et al., 1987). Other estimates are less extreme, suggesting mean annual temperatures of −9 °C at the margin of the ice sheet in central Scotland (Glasser and Siegert, 2002), or − 7 °C in south-east England during the late Pleistocene (Coope et al., 1971). Based on these studies, Westaway and Younger (2013) derived temperature histories for the previous 150 ka, within which temperatures at the time of the LGM were estimated to be 18 °C and 20 °C lower than those at present for southern and northern Britain, respectively. A global reconstruction of temperature changes at the LGM suggested mean annual air temperature of −5 °C to −6 °C across the UK (Annan and Hargreaves, 2013), however the uncertainty is large ranging from 4 to 8 °C across southern England and 8–20 °C across northern England and Scotland.

We applied a similar approach using a global proxy record to generate temperature projections. To take into account the large uncertainty in past surface temperatures across Great Britain, we adopted a method based on the use of a set of four different scenarios of the temperature history over the last 1 million years. In order to estimate the cyclicity of the temperature time-series, a Pliocene-Pleistocene stack of 57 globally distributed benthic $\delta^{18}O$ (Fig. 2a) records was used to serve as an estimate of the shape of the temperature time-series (Lisiecki and Raymo, 2005). The fluctuations of North hemisphere surface air temperature and the benthic $\delta^{18}O$ isotope record have been found to related closely (Bintanja et al., 2005). Each of the temperature time-series is constructed by linearly scaling the global $\delta^{18}O$ time-series, considering a present day annual air temperature (T_0) of 8.5 °C, and a temperature offset (ΔT) in the resulting four scenarios of −10, −14, −18, and − 25 °C below the present temperature at the time of maximum $\delta^{18}O$. The temperature T_t at time t is described in Eq. (1), where $\delta^{18}O_0$ is the $\delta^{18}O$ at

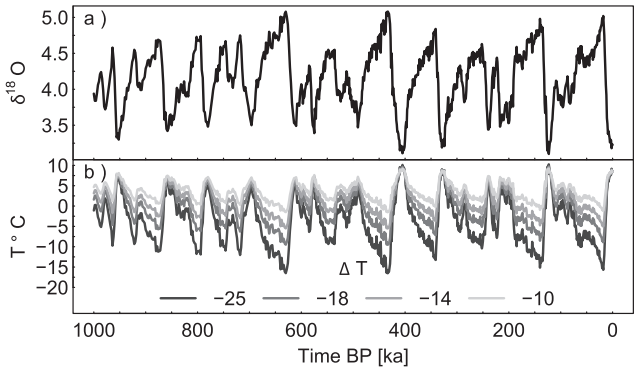

Fig. 2. a) Global $\delta^{18}O$ time-series after Lisiecki and Raymo (2005) and b) scaled surface temperature time-series using ΔT ranging from −10 to −25 °C.

present day, and $\delta^{18}O_t$ the δ^{18}O at time t. The resulting temperature scenarios are shown in Fig. 2b.

$$T_t = \frac{\delta^{18}O_t - \delta^{18}O_0}{\max\left(\delta^{18}O_t - \delta^{18}O_0\right)}\Delta T + T_0 \quad (1)$$

2.2.2. Geothermal heat flux

Geothermal heat flux data were originally collated, along with data on subsurface temperature, thermal conductivity and geochemistry, and catalogued as part of a project commissioned by the UK Department of Energy and the European Commission between 1976 and 1988 (Burley and Edmunds, 1978). This catalogue has since been updated in three revisions (Burley and Gale, 1982; Burley et al., 1984; Rollin, 1987). A UK heat flow map has been derived from 212 heat flow measurements augmented by 504 heat flow estimates (Downing and Gray, 1986; Rollin, 1995; Busby et al., 2011). This map shows a fairly uniform background field with areas of increased heat flow associated with radiogenic granites (Busby and Terrington, 2017), and has been used to define heat flux boundary conditions at the base of the models in this study. Recently a revised heat flow map has been published (Busby and Terrington, 2017), applying paleoclimatic and topographic correction of heat flow, resulting in a higher heat flux of approximately 16 mW m^{-2} to regions north of the southern extent of the Devensian ice at the Last Glacial Maximum and 20 mW m^{-2} south of the ice extent (Busby and Terrington, 2017).

2.3. Soil freezing and relative hydraulic conductivity functions

To simulate heat advection in a groundwater system undergoing freezing and thawing, two functional relationships must be defined: (i) the 'soil freezing' function, describing the relationship between temperature and ice saturation; and (ii) the relative hydraulic conductivity function describing the relationship between relative hydraulic conductivity and ice saturation.

Experimental data for soil freezing and relative hydraulic conductivity functions are limited to sands, silts and clays (e.g. Burt and Williams, 1976; Kleinberg and Griffin, 2005; Watanabe and Flury, 2008; Azmatch et al., 2012). The soil freezing curve for different soil types can be fundamentally different. The choice of freezing function used in numerical models should be smooth and easily differentiated, since the derivative is used to calculate the apparent heat capacity (McKenzie et al., 2007). Here, we use a smoothed Heaviside function (see Appendix A) with a freezing interval from 0 °C to −1 °C, which Scheidegger et al. (2017) show is similar to other previously used freezing curves.

Model descriptions of how the hydraulic conductivity decreases over the freezing interval commonly assume an analogue to unsaturated fluid flow and the relationship between moisture content and suction described by a soil water retention curve (McKenzie et al., 2007; Kurylyk and Watanabe, 2013). Other coupled groundwater flow and permafrost models use a linear decrease in relative hydraulic conductivity with temperatures between freezing and the temperature at which the residual saturation is reached, or an impedance factor law for which the minimum hydraulic conductivity is limited (McKenzie et al., 2007). A minimum value of relative hydraulic conductivity in permafrost of 1e-6 has been suggested as an arbitrary small minimum value (McKenzie et al., 2007).

For numerical modelling a relative hydraulic conductivity of permafrost of six orders of magnitudes lower has been applied by several groups (McKenzie et al., 2007; Ge et al., 2011; Grenier et al., 2013) either using an exponential decrease in relative hydraulic conductivity or a linear decrease. Other minimum relative hydraulic conductivities applied to coupled numerical models are 1e-8 (Bense et al., 2009), or an absolute hydraulic conductivity of 1e-33 [m s^{-1}] for what is termed an impermeable permafrost case (McKenzie and Voss, 2013). For a higher hydraulic conductivity permafrost case, a linear function decreasing six orders of magnitudes has been previously used, which was suggested is likely to exaggerate the ease of groundwater flow though frozen media (McKenzie and Voss, 2013).

In this study we used the relative hydraulic conductivity, k_{rw}, function of Hansson et al. (2004):

$$k_{rw} = 10^{-S_i\Omega} \quad (2)$$

where S_i is the ice saturation and Ω a scaling parameter. Because of the limited availability of relative hydraulic conductivity functions measured for sand, silt and clays, and their absence for hard rocks, we varied Ω between 6, 3 and 1, which results in a decrease in relative hydraulic conductivity of six, three and one order of magnitude, respectively.

2.4. Modelling methodology

We applied a numerical model to simulate groundwater flow, heat transport and permafrost dynamics across the two geological settings. Whilst the model simulates a number of state variables of the system, our objective was to investigate the development of permafrost. Specifically, we aimed to simulate permafrost thickness (*PF*), which we define as the distance between the land surface, from which permafrost develops downwards, and the lowest point at which the ice saturation is greater than zero; this point is equivalent to the 0 °C isotherm. Permafrost thickness varies laterally across the two settings, and in time. However, the principal focus of this study was to estimate the maximum permafrost thickness, PF_{max}, over glacial cycles.

2.4.1. Numerical solution of coupled flow, heat transport and permafrost dynamics

We applied the advection-diffusion equation including latent heat of fusion to model permafrost and groundwater flow. Groundwater flow and permafrost development are coupled using a hydraulic conductivity that is several orders of magnitude lower in frozen than under unfrozen conditions, and through a source term that is related to volume changes between ice and water. Heat flow is coupled to groundwater flow through the advective heat flow term, which is proportional to Darcy flow. A full description of the underlying model equations is given in Appendix A, which were solved within the COMSOL Multiphysics mathematical modelling environment (COMSOL, 2016) using the finite element method and its multifrontal massively parallel sparse (MUMPS) direct solver and a damped version of Newton's method to handle parameters. Grenier et al. (2018) showed that simulations made with COMSOL Multiphysics for a number of groundwater flow and permafrost benchmark problems agreed closely to those made with other similar software codes.

We also applied 2D cross-sectional and vertical 1D models to simulate permafrost dynamics considering conduction but not advection of heat (thus removing the second term on the left hand side of Eq. (A.1)). These faster-running 1D models were used to perform large-ensemble sensitivity analyses.

2.4.2. Model set-up

We constructed 2D slice (x-z) finite element models of the two settings using COMSOL Multiphysics. The model domain for GS1 is shown in Fig. 1a. The model is 20 km long and extends to a depth of 2 km below sea level, which is taken as the datum. The domain was discretised using a structured quadrilateral finite-element mesh. In the top 800 m the vertical mesh spacing is 5 m, and below this it is 25 m. The horizontal mesh spacing is 100 m. The right-hand boundary is closed to both heat and fluid flow, as this represents a topographic high at 920 meters above sea level (m asl), and a groundwater divide. A constant groundwater head boundary condition is defined at the left-hand boundary representing sea level. Heat leaves the left-hand boundary through advection. At the upper boundary, a Dirichlet

Table 1
Thermal and hydraulic properties for GS1: rock thermal conductivity (λ_r), rock mass heat capacity (C), porosity (ε), density (ρ), horizontal hydraulic conductivity (K_x), vertical hydraulic conductivity (K_z) and aquifer specific storage (S_s).

Layer	λ_r [W m^{-1} K^{-1}]	C [J kg^{-1} K^{-1}]	ρ [kg m^{-3}]	ε [−]	K_x [ms^{-1}]	K_z [ms^{-1}]	S_s [m^{-1}]
1. Weathered sandstone	3.1	850	2650	0.12	3.16e-6	K_x	1e-4
2. Upper sandstone	3.1	850	2650	0.15	1e-6	K_x/10	1e-4
3. Lower sandstone	3.1	850	2650	0.075	1e-7	K_x/10	1e-4
4. HSR (quartzite or meta-lava)	4	850	2650	0.001	1e-9	K_x	1e-6
5. Weathered HSR (quartzite or meta-lava)	3.1	850	2650	0.05	3.16e-6	K_x	1e-6

boundary condition is specified and the hydraulic head is set to the elevation of the land surface; this is an assumption that we recognise is uncertain, but which has been commonly applied previously (e.g. Bense et al., 2012; McKenzie and Voss, 2013) given the difficulties of alternatively specifying recharge boundaries in permafrost environments. The temperature is also specified at the upper boundary, the details of which are discussed in the next subsection. The base of the model is closed to fluid flow, but heat enters the model domain by conduction, by applying a geothermal heat flux as a Neumann boundary condition. The model consists of five lithological units representing: (1) weathered sandstone at the surface, overlying (2) upper and (3) lower sandstones above (4) HSR (quartzite or meta-lava), which is (5) weathered where it outcrops. Within each unit physical properties and, therefore, model parameters are homogeneous. Hydraulic properties for the five units were taken from Towler et al. (2008), and thermal properties from McKeown et al. (1999); these are listed in Table 1. Towler et al. (2008) presented ranges of values for hydraulic conductivity and we took the upper bound of these, thereby investigating the case where flow and heat advection would be most significant.

The model domain for GS2 is shown in Fig. 1b. The model is 300 km long and extends to a depth of 1.5 km below sea level. The land surface rises to 170 m at the right-hand boundary, thus the topographic gradient is relatively low (~0.06%). The domain was discretised using a vertical mesh spacing of 5 m to a depth of 500 m, and 25 m below this; the horizontal mesh spacing was 1000 m. The lateral boundaries are closed to both fluid and heat flow. At the base of the model there is no fluid flow, but an upward heat flux was applied. Along the upper boundary, the hydraulic head is set to the elevation of the land surface, where a temperature time-series, described below, was applied. The model represents the synclinal basin structure described above, composed of a sedimentary sequence overlying igneous HSR, categorised into nine lithological units (Fig. 1b). Hydraulic properties for the different lithological units are again taken from Towler et al. (2008) and represent the suggested maximum hydraulic conductivities, and thermal properties from Rollin (1987); these are listed in Table 2. Parameters specifying the thermo-hydrogeological properties within the model are listed in Tables 1–3 and Appendix A.

The temperature series derived by scaling the global $\delta^{18}O$ time-series are applied uniformly over the upper, land surface boundaries of the 2D models of the two geological settings. At the base of the two 2D models, a geothermal heat flux (W m^{-2}) is defined based on heat flow data for Great Britain (Busby et al., 2011). The geothermal heat flux across the UK is locally variable but principally determined by the vertical geological sequence. The heat flux applied across the bottom boundaries of the models is 70 mW m^{-2} for G1 and 55 mW m^{-2} for GS2.

2.4.3. Initial conditions

The initial conditions for temperature and hydraulic head were derived in two steps: first a steady-state simulation was run with temperature at the land surface set to that at $t = 123$ ka, and hydraulic head along the same boundary set to the topographic elevation. Second, a transient simulation was run with the same hydraulic head boundary condition but using the surface temperature time-series from 123 ka to present. The resulting temperature and hydraulic head field were then used as an initial condition for the model simulations.

2.4.4. Model simulations

Four series of simulations were performed to calculate the range of maximum permafrost thickness values that could occur over glacial time-scales. The individual model runs within each of these series are described next and listed in Table 4.

2.4.5. Effect of surface temperatures

In this series of four simulations (ST_10, 14, 18, 25), the four surface temperature time-series were applied to each of the 2D models of GS1 and GS1 (Fig. 1; Tables 1–4) to quantify the impact of progressively colder surface temperatures on permafrost thickness. The Ω parameter in Eq. (2) was set to 6 i.e. relative hydraulic conductivity reduces rapidly as ice saturation increases.

2.4.6. Influence of heat advection

In this series of three simulations (HA_1, HA_3, HA_6) of the 2D model of GS1, the influence of heat advection on permafrost thickness was investigated by setting the Ω parameter of the permafrost relative hydraulic conductivity function (Eq. 2) to either 1, 3 or 6. A higher value of Ω results in a more rapid decrease in relative hydraulic conductivity as ice saturation increases. Values of Ω of >6 were not used, as it was expected that this would produce very little difference in model results, which proved to be the case.

2.4.7. Comparison of 2D and 1D models

This series of four simulations was performed to quantify the differences between permafrost thickness at L1 (GS1) and L2 (GS2) when simulated using (i) the 2D models including groundwater flow and

Table 2
Thermal and hydraulic properties for GS2: rock thermal conductivity (λ), rock mass heat capacity (C), porosity (ε), density (ρ), horizontal hydraulic conductivity (K_x), vertical hydraulic conductivity (K_z) and aquifer specific storage (S_s).

Layer	λ_r [W m^{-1} K^{-1}]	C [J kg^{-1} K^{-1}]	ρ [kg m^{-3}]	ε [−]	K_x [ms^{-1}]	K_z [ms^{-1}]	S_s [m^{-1}]
1. Chalk	1.67	880	2200	0.1	1e−10	K_x	1e-4
2. Limestone	1.3	920	2400	0.25	1e-9	K_x	1e-4
3. Clay	1.3	920	2400	0.2	1e-9	K_x	1e-4
4. Limestone	2.23	840	2500	0.1	1e-5	K_x	1e-4
5. Mudstones/shales	1.3	820	2400	0.15	1e-12	K_x/10	1e-4
6. Mudstones/siltstones	2.07	920	2520	0.15	1e-10	K_x/10	1e-4
7. Sandstones	3.1	840	2550	0.1	1e-6	K_x	1e-4
8. HSR (granitic rock)	2.38	850	2500	0.15	1e-8	K_x	1e-4
9. HSR (basic igneous rock)	3.3	859	2630	0.05	1e-9	K_x	1e-6

Table 3
Physical properties of water and ice: thermal conductivity (λ), heat capacity (*C*), density (*ρ*) and latent heat of fusion (*Lf*).

Layer	λ [W m^{-1} K^{-1}]	*C* [J kg^{-1} K^{-1}]	*ρ* [kg m^{-3}]	*Lf* [J kg^{-1}]
Water	0.6	4182	1000	3.34e5
Ice	2.14	2060	920	3.34e5

heat advection; (ii) the 2D models using the same set-up and parameterisation as (i) including heat conduction but not groundwater flow and heat advection; and (iii) a 1D model of the each of the vertical geological profiles at L1 and L2 considering vertical heat conduction only. All models simulate phase changes between water and ice. The models were compared for the two surface temperature scenarios Δ*T-14* and Δ*T-25*. The 1D and 2D heat conduction-only models were also constructed in COMSOL Multiphysics. The purpose of these simulations was to investigate the role of heat advection in controlling PF_{max}.

2.4.8. Sensitivity to physical properties

In this series, multiple simulations of the 1D model driven by the Δ*T-14* surface temperature time-series were performed. In a first sequence in the series, thermal and hydraulic properties were set to those for each of the lithological units in GS1 and GS2. The thermal conductivity of frozen ground, λ_e, and the geothermal heat flux, q_{heat}, were then varied independently to assess the effect on simulated PF_{max}. The second sequence of runs were more generic, removing the link to the geological settings, and in which the rock thermal conductivity, λ_r, porosity, ε, and geothermal heat flux were varied independently. When varying one of these three parameters the other two were fixed to either low, medium, or high values from the following ranges: λ_r from 1.3 to 4.6 W m^{-1} K^{-1}; ε from 0.01 to 0.4; and q_{heat} from 36 to 136 mW m^{-2}. These ranges were selected to span plausible values for the different lithologies of the UK based on collated data (Busby et al., 2011; Rollin, 1987). This provided an estimate of the relative influence of thermal conductivity, geothermal heat flux and porosity on the maximum permafrost thickness, considering the uncertainty in the parameter values for GS1 and GS2. In a final sequence in the series, the sensitivity of PF_{max} to the temperature offset, Δ*T*, used to generate the surface temperature scenario, was investigated. The different surface temperature series were applied to each of eight models with different λ_r, ε, and q_{heat} values, based on the different combinations of the lower and upper values of the ranges specified for these parameters above.

To compare the effect of varying different parameters on permafrost thickness, we calculated the relative sensitivity (RS) of PF_{max} to the surface temperature scenario, and parameters describing hydrogeological properties, thermal properties and heat flow, and the permafrost relative hydraulic conductivity function. This is defined as:

$$RS = \left| \frac{\Delta PF_{max}/PF_{max}}{\Delta y/(y_{max}-y_{min})} \right|$$

where Δ*y* is the change in the parameter for which RS is calculated, y_{min} and y_{max} define the full range over which *y* is varied, and ΔPF_{max} is the change in PF_{max} over Δ*y*.

Table 4
Model runs for the 2D coupled models: in the ST series, applied to both GS1 and GS2, the scaled surface temperature time-series differs. In the HA series the frozen hydraulic conductivity of the permafrost, affecting heat advection, is modified by adjusting Ω (Eq. 2).

Runs	Δ*T*	Ω	GS
ST_10	−10	6	1,2
ST_14	−14	6	
ST_18	−18	6	
ST_25	−25	6	
HA_1	−14	1	1
HA_3	−14	3	
HA_6	−14	6	

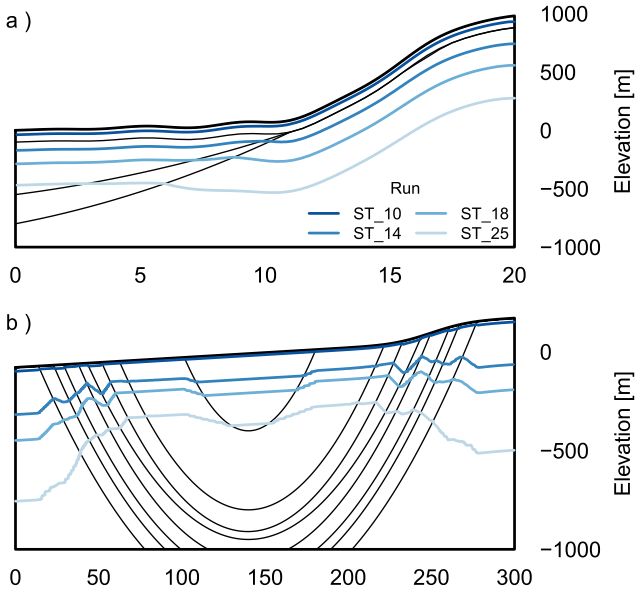

Fig. 3. Maximum permafrost thickness, PF_{max}, for GS1 and GS2 using the Δ*T-10*, *-14*, *-18* and *-25* °C surface temperature time-series.

3. Results

3.1. Effect of surface temperatures

The maximum modelled permafrost thickness, PF_{max}, for GS1 and GS2 is presented in Fig. 3. For GS1, PF_{max} generally follows the topography, but the thickness is greater in the HSR than in the sandstones, since the thermal conductivity is higher here (Table 1). The variation of PF_{max} for different lithological units is more pronounced for GS2, since there is a larger contrast in thermal conductivity between the different units (Table 2). Thickest permafrost is found in the HSR (239 m for ST_14) and thinner permafrost in the sequence of mudstones and siltstones (100 m for ST_14).

The time-series of simulated permafrost thickness at L1 (GS1) and L2 (GS2) are presented in Fig. 4. Deeper permafrost is modelled at L1 than L2 considering the same temperature scenario. This is because the lithological units in GS1 broadly have a higher thermal conductivity than those in GS2, and the effect of higher thermal conductivity outweighs here the effects of a lower geothermal heat flux in GS2 (55 versus 70 mW m^{-2}). During one glacial cycle, permafrost forms slowly and reaches a maximum depth towards the end of the glacial cycle, when permafrost thaw occurs over a relatively short time-scale of a few

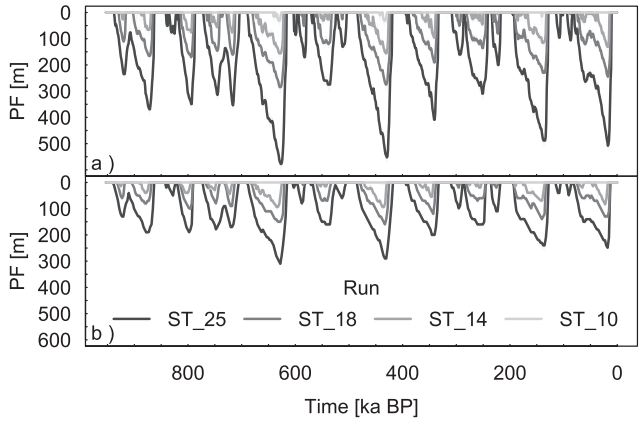

Fig. 4. Permafrost thickness at a) L1 (GS1) and b) L2 (GS2) using the four scaled surface temperature series of Fig. 2b.

Table 5
Variation in PF_{max} (m) at L1 (GS1) and L2 (GS2) when permafrost is defined using different ice saturations, S_i.

S_i	L1				L2			
	ΔT-25	*ΔT-18*	*ΔT-14*	*ΔT-10*	*ΔT-25*	*ΔT-18*	*ΔT-14*	*ΔT-10*
>0	597	310	175	51	320	160	104	10
0.5	578	285	156	31	310	150	94	0
0.95	553	270	141	16	290	140	84	0

thousand years. For example, for run ST_14 for L1, permafrost thawed after the last glacial cycle over three thousand years, whereas it formed over 19 thousand years. The maximum modelled permafrost thickness at L1 ranges between 51 m for ST_10 to 597 m for ST_25. At L2 the maximum permafrost thickness ranges between 10 m for a ST_10 and 320 m for ST_25 (Table 5). As a large proportion of the permafrost can be unfrozen or consist of a low ice saturation, it is important to differentiate between permafrost depth and the frozen depth. In the ST series of runs, the frozen depth was simulated to be up to 44 m shallower than the permafrost depth (Table 5, GS1, ST_25). The degree of ice saturation in the model depends on the latent heat of freezing and thawing water within the rock.

The number of simulated permafrost events occurring during the past 1 million years at different depths varies for the different temperature time-series and for the different geological settings (Table 6). For example, at L1, there are two permafrost events reaching a depth of 500 m for run ST_25, whereas at L2 the permafrost reaches a depth of 300 m once for ST_25. For ST_14, the maximum permafrost depth does not reach 200 m, but reaches a depth of 100 m seven times at L1 and twice at L2.

3.2. Influence of heat advection

The influence of heat advection on the permafrost thickness is modelled to be up to several tens of meters locally for GS1. Heat advection in GS1 is high, as the hydraulic conductivity of the weathered layers and the sandstone is high and the hydraulic gradient is large (Fig. 5a and b). During the time of maximum permafrost thickness (628 ka BP), the permafrost thickness across the model domain is relatively uniform for the scenario in which permafrost has a low hydraulic conductivity (HA_6, $\Omega = 6$) (Fig. 5a). However, for the scenario in which permafrost has a higher hydraulic conductivity (HA_1, $\Omega = 1$), permafrost is significantly thinner beneath discharge points. During a time of permafrost thawing, at 14 ka BP, the difference between runs HA_6 and HA_1 is more pronounced (Fig. 5b); the permafrost has a relatively uniform thickness for HA_6, but is more variable for HA_1 due to thawing of permafrost by head advection at discharge points.

For HA_1, groundwater recharge is reduced at the time of maximum permafrost thickness (Fig. 5c), but since the hydraulic conductivity of the permafrost is lowered by only one order of magnitude, some recharge still takes place. This results in a hydraulic head field similar to that occurring when the domain is unfrozen; differences in hydraulic heads occur around the discharge points, and beneath the high ground where they decrease by approximately 50 m. The high hydraulic gradient results in some heat advection, resulting in a non-uniform permafrost thickness. During permafrost thaw (Fig. 5d), the effect of heat advection is large enough to create a talik 7 km from the left-hand boundary, into which groundwater discharges. Downwelling of cold water from the interfluve in the higher hydraulic conductivity permafrost case (Fig. 5c and d) creates thicker permafrost compared to the low hydraulic conductivity permafrost case (Fig. 5e and f).

For HA_6, the hydraulic conductivity of the permafrost reduces by six orders of magnitudes and recharge reduces accordingly when permafrost forms. As a result, hydraulic heads drop to near zero beneath the permafrost at the time of maximum permafrost thickness, and heat advection does not influence the permafrost distribution (Fig. 5e). During permafrost thaw, and when permafrost does not extend to beneath the weathered layer, some recharge takes place and hydraulic heads rise over a relatively short time-scale of approximately 2 ka (Fig. 5f).

Fig. 6 compares the permafrost thickness time-series at L1 and L2 simulated using the 1D conduction-only, 2D conduction-only, and 2D conduction-advection models (HA_6 and HA_1) driven by the *ΔT-14* and *ΔT-25* surface temperature series. Generally, the time-series of permafrost thickness simulated by the 1D model is smoother than that of the 2D conduction-only model, since the mesh size for the 1D model is 1 m and for the 2D model is 5 m in the vertical. Otherwise, the time-series are similar.

At L1, with *ΔT-14*, PF_{max} is 35 m greater for HA_1 than the 2D conduction-only model, a difference of approximately 25%, however there are no differences in PF_{max} between the HA_6 and the 2D conduction-only models (0 m). HA_1 results in thicker permafrost than HA_6 and the conduction models when it is shallower. However, when permafrost is deep, i.e. extending beneath the lower sandstone, e.g. in T-25, permafrost thicknesses simulated by the 2D conduction-only, HA_6 and HA_1 models are similar (differences are <10 m, or < 2%).

At L2, the differences between the four models are generally less. For *ΔT-14* and *ΔT-25*, PF_{max} is 1.5 and 7.5 m higher, respectively, in the 1D than the 2D conduction-only model, a difference of approximately 1% or 3%; it is 0 m and 5 m higher in the 2D conduction-only than the HA_1 model, a difference of approximately 0% or 2%. In GS2 the hydraulic conductivity of the rock is low and heat advection has a negligible influence on the permafrost thickness.

Differences in PF_{max} at L1, simulated by the 1D and HA_6 models, are 4 m and 8 m for the *ΔT-14* and *ΔT-25* scenarios, respectively. At L2 the differences between these two models are 13 m and 2 m, again for the *ΔT-14* and *ΔT-25* scenarios, respectively. These differences are contributed to by the fact that permafrost thickness is calculated using a discretised mesh of solution points, the spacing of which is approximately 5 m. The difference in PF_{max}, between the 1D conduction-only and HA_1 models with *ΔT-25* is 14 m and 13 m (3% and 5% of PF_{max}), for L1 and L2, respectively. These results indicate that, if that it is considered that $\Omega = 6$ in Eq. (2), then it can be assumed that a 1D conduction-only models will provide a good estimate of PF_{max}.

Table 6
Number of permafrost events at different depths, and maximum duration in ka of a permafrost event (in brackets) at L1 (GS1) and L2 (GS2). No events for grey cells or *ΔT-10* scenario.

	L1			L2		
Depth (m)	*ΔT-25*	*ΔT-18*	*ΔT-14*	*ΔT-25*	*ΔT-18*	*ΔT-14*
100	19 (70)	16 (56)	6 (20)	13 (62.5)	6 (37.5)	2 (5)
200	13 (59)	5 (31)		5 (37.5)		
300	11 (46)	1 (4)		1 (5)		
400	6 (32)					
500	4 (17)					

3.3. Sensitivity to physical properties

As described above, PF_{max}, was simulated using the 1D model driven by the *ΔT-14* surface temperature time-series, in a series of runs based on the properties of the lithological units that comprise GS1 and GS1 (Tables 1 and 2), but where either the thermal conductivity of the frozen ground, λ_e, or the geothermal heat flux, q_{heat}, was varied. The plots of PF_{max} against λ_e and q_{heat} are shown in Fig. 7. Lithologies with low thermal conductivities (mudstones, siltstones, shales and chalk) generate the lowest permafrost thickness whilst HSR with high thermal conductivities generate the thickest permafrost (Fig. 7a). The relationship

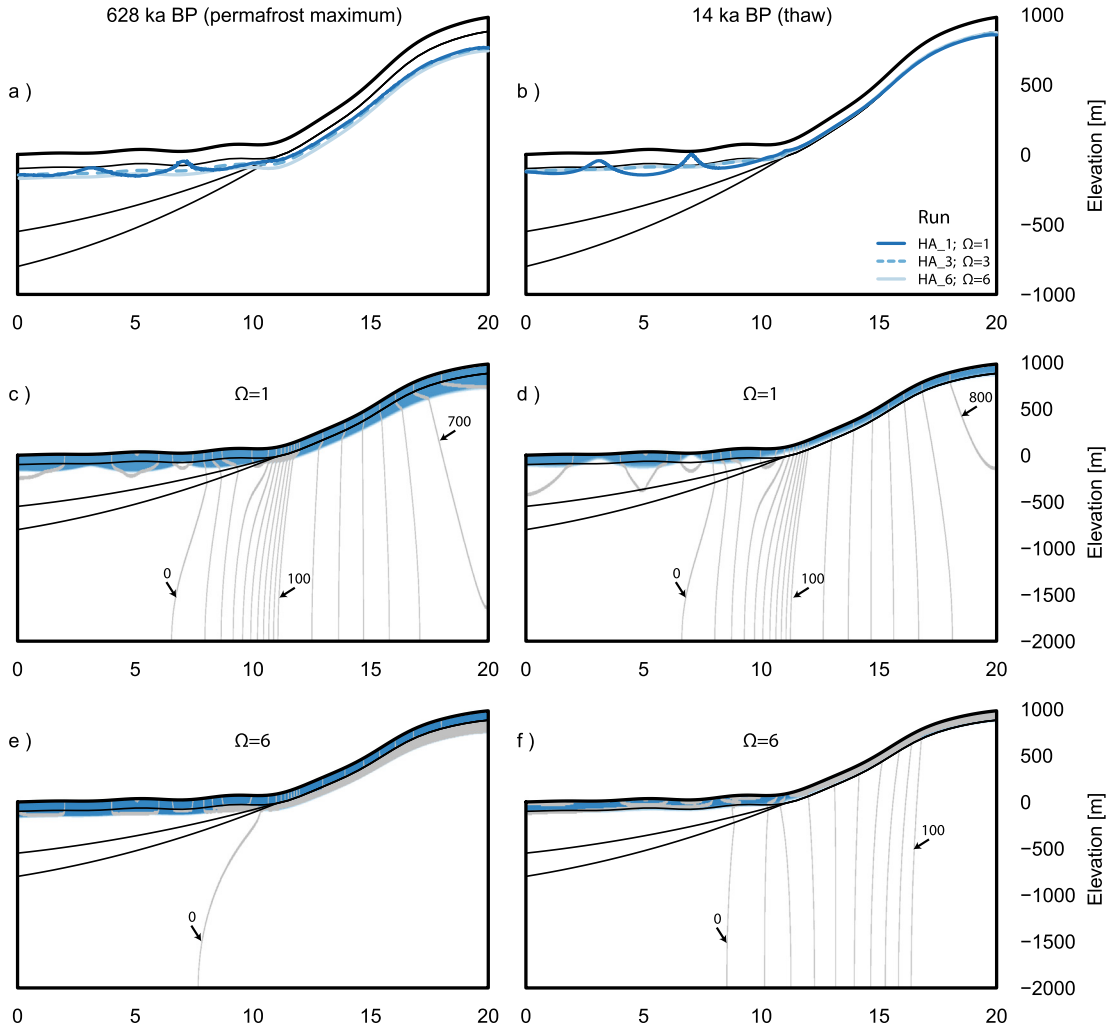

Fig. 5. Results from simulations of GS1 at time of maximum permafrost, 628 ka BP (left-hand column), and a time of thaw, 14 ka BP (right-hand column). Figures a & b compare simulated permafrost thickness using $\Omega = 1$, 3, and 6. Figures c & d show the permafrost distribution (blue) and hydraulic head contours (grey) using $\Omega = 1$. Figures e & f show the same but with $\Omega = 6$. Note the head contour intervals vary and are 10 m and 100 m below and above the 100 m contour line, respectively.

between the thermal conductivity of the frozen ground and the maximum permafrost thickness is approximately linear but complicated by the fact that the units have different porosities, and thus different magnitudes of latent heat dampening the temperature signal.

As expected, there is an inverse relationship between geothermal heat flux and PF_{max}. However, the change in PF_{max} as a function of q_{heat} depends on the thermal properties. For the highest value of λ_e (4 W m^{-1} K^{-1}, unit 5, GS1: HSR), varying the heat flux from 55 to 100 mW m^{-2} produces a 148 m decrease in PF_{max} from 347 to 199 m. However, for the lowest value of λ_e (1.3 W m^{-1} K^{-1}, unit 5, GS2: mudstones/shales), the same variation in heat flux results in a 45 m decrease in PF_{max} from 111 to 66 m. Similarly, PF_{max} is more sensitive to variations in geological properties (thermal conductivity, heat capacity, porosity) when the geothermal heat flux is low (Fig. 7b).

The sensitivity of PF_{max} to the rock matrix thermal conductivity, λ_r, porosity, ε, and geothermal heat flux, q_{heat}, was also investigated using the 1D model, again driven by the ΔT-*14* surface temperature time-series. In each case, the two other parameters were set to low, medium, and high values representative of values for lithological units in the UK. Variations in PF_{max} are plotted in (Fig. 8a–c). These simulations are similar to those performed to generate the results plotted in Fig. 7 but remove the influence of the variation in the porosity on the effective thermal conductivity of frozen ground. The relative sensitivities for each of the three parameters are presented in Fig. 8d–f.

It is evident that the deepest permafrost will occur where thermal conductivity is high, and porosity and geothermal heat flux are low. Under steady-state conditions permafrost thickness scales linearly with surface temperature, thermal conductivity and geothermal heat flux: $PF_{max} = T \times \lambda / q_{heat}$ (Williams and Smith, 1989). However, since no steady-state is reached using the ΔT-*14* temperature time-series, we do not expect this.

As for the results of the 1D model with properties based on the lithological units for GS1 and GS2, there is a positive relationship between rock thermal conductivity, λ_r, and PF_{max} (Fig. 8a). However, removing the effects of porosity results in a smoother relationship than that between λ_e and PF_{max} in Fig. 7. With the low values of porosity (0.01) and geothermal heat flux (36 mW m^{-2}), PF_{max} varies from 160 to 576 m for λ_r values of 1.5 and 4.5, respectively. With the high values of porosity (0.4) and geothermal heat flux (136 mW m^{-2}) PF_{max} varies from 52 to 108 m, across the same λ_r range. From Fig. 8a it is evident that uncertainty in λ_r has the largest effect where q_{heat} and porosity are low.

The relative sensitivity for λ_r (Fig. 8d) is larger for low thermal conductivity and decreases nonlinearly as thermal conductivity increases, under otherwise unchanged conditions. The spread in relative sensitivities is larger for lower thermal conductivity than for higher thermal conductivity. This can be explained by the thermal conductivity of the frozen ground, which has a larger spread for low porosity, since with increasing porosity the thermal conductivity tends towards that of ice.

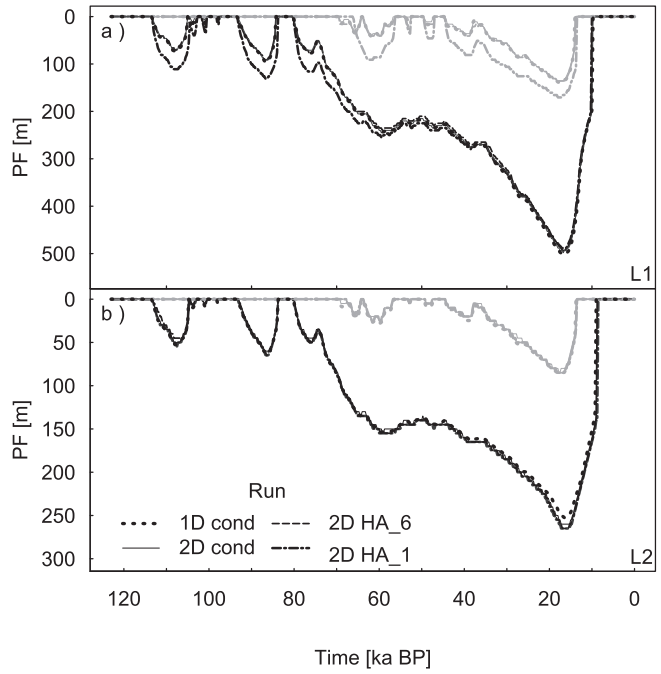

Fig. 6. Permafrost thickness at a) L1 (GS1) and b) L2 (GS2) simulated using the 1D conduction-only, 2D conduction-only, and HA_6 and HA_1 models, driven by Δ*T-14* (grey) and Δ*T-25* (black) surface temperatures.

Porosity is inversely related to permafrost thickness (Fig. 8b). There is a negative relationship between porosity and permafrost thickness when thermal conductivity is high and heat flow is low, with a range of permafrost thickness of 489 m, from 107 and 596 m. The main causes for this non-linearity are the transient effects of freeze-thaw. Porosity determines the amount the thermal properties change with freeze/thaw and release/uptake of latent heat. When water freezes, the thermal conductivity increases by a factor of approximately 3.5 and the mass heat capacity decreases by half. In addition, the energy required for water to freeze, or released when ice thaws, is equal to that required raising the temperature of an equal volume of rock by approximately 150 °C.

The relative sensitivity for porosity (Fig. 8e) is larger for higher thermal conductivity and lower geothermal heat flux values. Maximum *RS* values are approximately half of those for rock thermal conductivity and heat flux, and RS decreases to near zero with low λ_r.

The influence of the geothermal heat flux on PF_{max} also depends on the thermal conductivity and porosity (Fig. 8c). For the high thermal conductivity and low porosity values, the range of PF_{max} is 406 m: from 576 m for the low heat flux to 170 m for the high heat flux. In contrast, for a low thermal conductivity and a high porosity, the range of permafrost thickness is 91 m (52 to 143 m).

The spread of the relative sensitivity values for geothermal heat flux (Fig. 8f) are similar to that for thermal conductivity, though they would be of opposite sign if the absolute value was not considered. *RS* is largest for low porosity, since the relative importance of geothermal heat flux is dampened with higher porosity and associated latent heat effects. With increasing geothermal heat flux, the range between the maximum and minimum relative sensitivity values decreases. With a sufficiently high geothermal heat flux, the maximum permafrost thickness will tend towards zero.

The relationship between PF_{max} and the Δ*T* value used to scale the surface temperature series is shown in Fig. 9a, for eight models based on combinations of low and high values of λ_r, ε, and q_{heat}. This is near-linear when the thermal conductivity is large, and porosity and geothermal heat flux are low. With higher porosity and geothermal heat flux and lower thermal conductivity, the relationship is slightly curvilinear: PF_{max} increases by less as surface temperatures decrease. The relative sensitivity of PF_{max} to the Δ*T* scaling value (Fig. 9b) is largest for the warmest surface temperature scenarios, when permafrost is thin and when a small decreases in temperature results in a relatively large increase in permafrost thickness. For example, changing ΔT from −10 to −11 °C increases PF_{max} by 40–80%, whereas a change of ΔT from −24 to −25 °C increases it by 4–9%. However, the absolute change in permafrost thickness remains similar with change in ΔT of 1 °C.

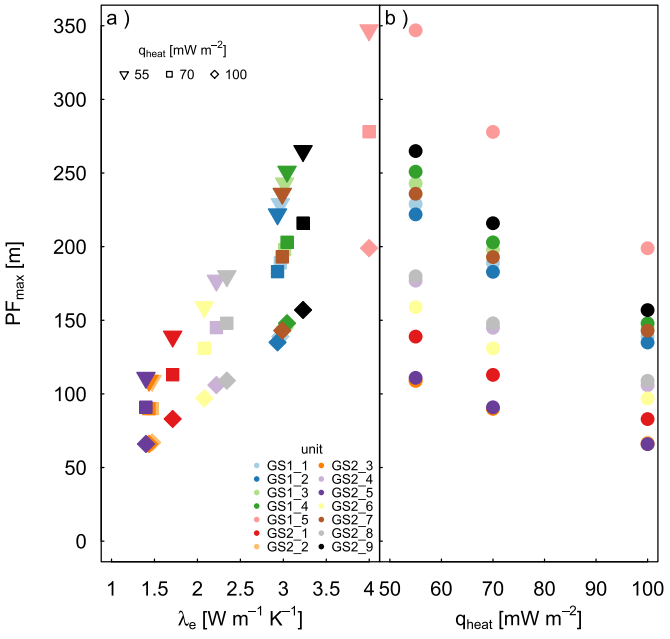

Fig. 7. PF_{max} as a function of a) thermal conductivity of frozen ground, λ_e, and b) geothermal heat flux, q_{heat}, for the Δ*T-14* surface temperature scenario. The colours correspond to the geological properties for the units 1–14 as listed in Table 1 and Table 2. The shape of the symbol represents geothermal heat flux applied (triangle: 55; square: 70; diamond: 100 mW m^{-2}).

4. Discussion

4.1. Sensitivity of physical properties and temperature forcing to maximum permafrost thickness

The modelling has shown how the maximum permafrost thickness depends on surface temperature forcing, thermal conductivity, geothermal heat flux, and porosity, and that the relative sensitivity of each variable is affected by the magnitude of the other variables. The relative sensitivity expresses the proportional change in PF_{max} for a proportional change in a parameter with respect to the range over which it could potentially vary. The range of calculated relative sensitivities of PF_{max} to the adjusted variables are summarised as box-and-whisker plots in Fig. 10. PF_{max} is most sensitive to the Δ*T* surface temperature scaling, then to the geothermal heat flux, thermal conductivity, porosity, and the parameter controlling the permafrost hydraulic conductivity. It is therefore the uncertainty in the surface boundary condition that contributes most significantly to the uncertainty in the simulated maximum permafrost thickness; PF_{max} ranges were 51 to 597 m for GS1 at L1, and 10 to 320 m for GS2 at L2, for the Δ*T* scaling range of −10 to −25 °C.

The full suite of 1D models produced *RS* values for Δ*T* of between 0.8 and 6.5. However for the two geological settings these ranges were 1.0 to 2.7 (GS1), and 1.0 to 3.4 (GS2). As illustrated in Fig. 9, the relative sensitivity of PF_{max} to Δ*T* decreases as Δ*T* becomes more negative (i.e. as surface temperatures cool). For example, shifting from the Δ*T-14* to the Δ*T-18* scenario resulted in PF_{max} increasing by 77 and 55% in GS1

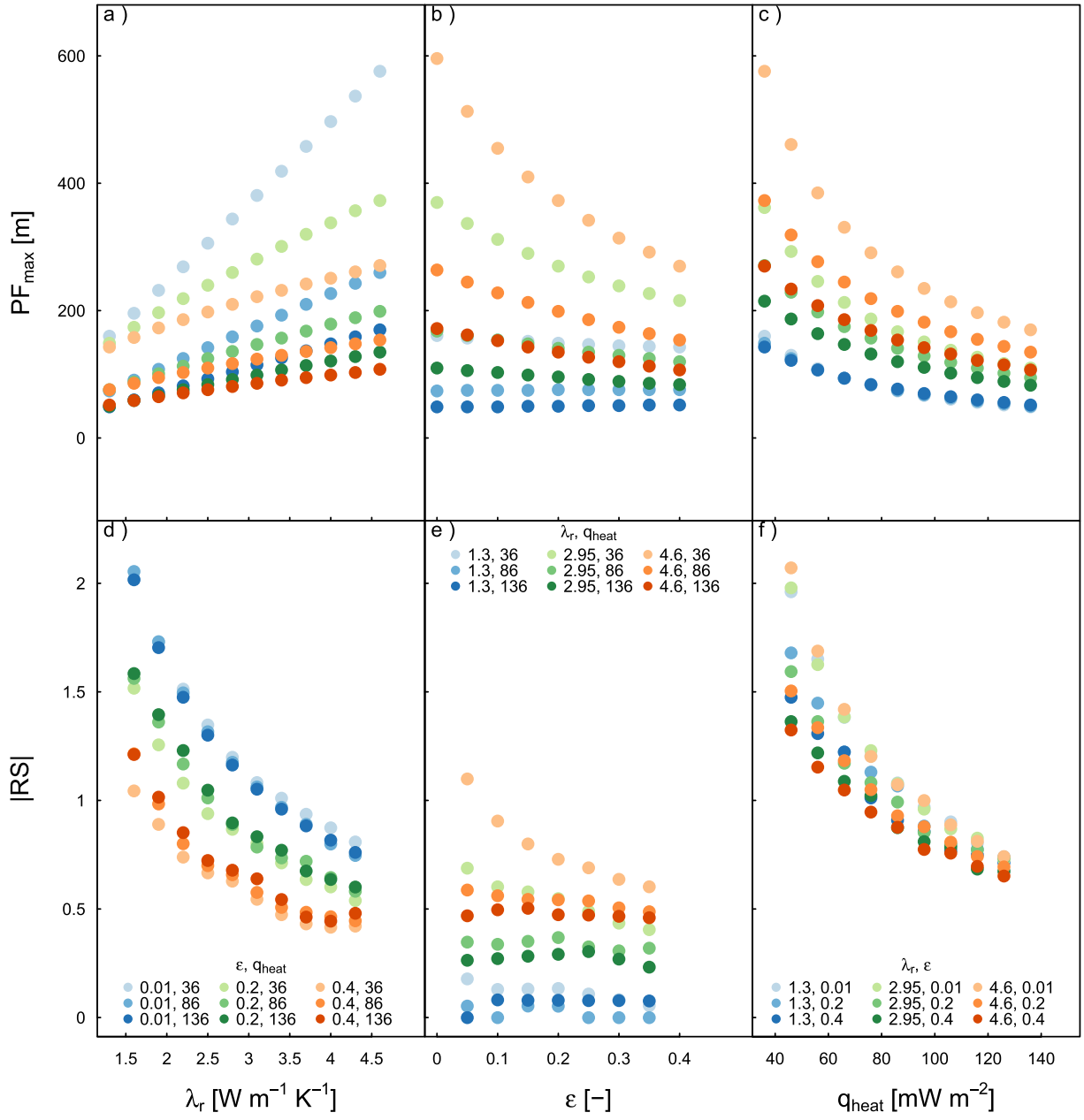

Fig. 8. PF_{max} (a–c), and relative sensitivity of maximum permafrost thickness (d–f), as a function of thermal conductivity λ_r, porosity ε, and geothermal heat flux, q_{heat}, for the ΔT-*14* surface temperature scenario. The values of the two other parameters for each vertical pair of figures are given in the legend.

and GS2, respectively, whereas shifting from ΔT-*18* to the ΔT-*25* resulted in increases of 93 and 100%, respectively.

The thermo-hydrogeological properties of the two geological settings are contrasting, with GS1 representing a broadly higher hydraulic and thermal conductivity system. It also has a 27% higher geothermal heat flux. This results in significantly different simulated values for PF_{max}. For example, PF_{max} is 41 m thicker at L1 (GS1) than at L2 (GS2), for the ΔT-*10* scenario, and 277 m thicker in the ΔT-*25* scenario.

There is a positive relationship between thermal conductivity and maximum permafrost thickness; larger permafrost thicknesses are expected in units with high thermal conductivity such as the HSR. For porosity and geothermal heat flux there is a negative relationship with PF_{max}. However, the effect of each parameter depends on the magnitude of the other properties values. For example, the maximum impact of a change in thermal conductivity on the permafrost thickness occurs where porosity and geothermal heat flux are low, and the smallest impact occurs where porosity and geothermal heat flux are large. Similarly, a variation in geothermal heat flux has the largest effect on the maximum permafrost thickness where thermal conductivity is large and porosity is low.

Considering the ΔT-*14* surface temperature scenario, the maximum amount by which the simulated PF_{max} value could vary was found to be 430 m (Fig. 8a–c) when the following properties were sampled across their plausible ranges as follows: λ_r is varied between 1.3 and 4.6 W m^{-1} K^{-1}, ε between 0.01 and 0.4; and q_{heat} between 36 and 136 mW m^{-2}. Varying one parameter at a time within these ranges, the simulated PF_{max} was found to vary as follows:

- λ_r varied between 1.3 and 4.6 W m^{-1} K^{-1}; PF_{max} variation of 56 m/566 m when ε set to its low/high value; q_{heat} set to its low/high value.
- ε varied between 0.01 and 0.4; PF_{max} variation of 3 m/305 m when λ_r set to its low/high value; q_{heat} set to its high/low value.

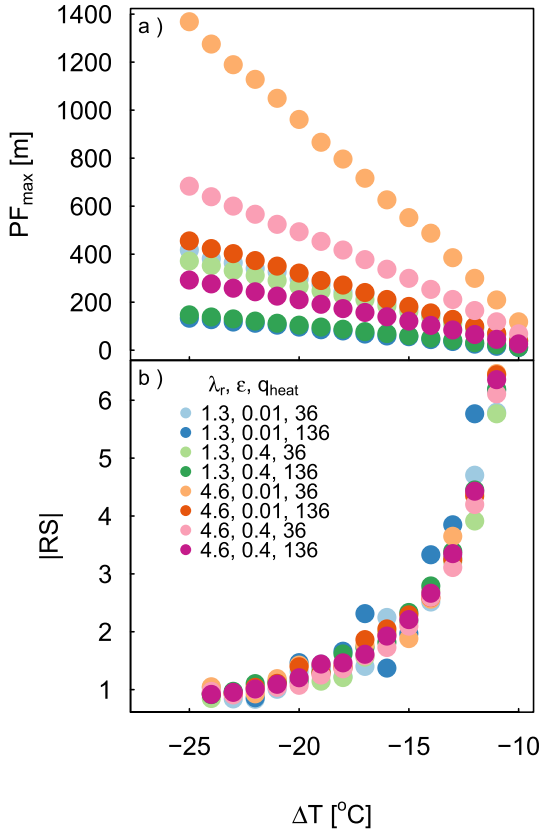

Fig. 9. PF_{max} as a function of the ΔT value used to scale the surface temperature series, and relative sensitivity of PF_{max} to the ΔT simulated using the 1D model. λ_r, ε, and q_{heat} set to the lower and upper limits of plausible values.

- q_{heat} varied between 36 and 136 mW m^{-2}; PF_{max} variation of 91 m/416 m when ε set to its high/low value; λ_r set to its low/high value.

The spread of simulated relative sensitivity, *RS* for rock thermal conductivity (0.4 to 2) and geothermal heat flux (0.7 to 2) are comparable, with the relative sensitivity for thermal conductivity and geothermal heat flux being highest for low porosities. The largest effect of a change in porosity occurs where the thermal conductivity is large, and geothermal heat flux is low; for the *ΔT-14* scenario, simulated PF_{max} was found to vary by up to 330 m when sampling the porosity across its plausible range of values. The relative sensitivity, *RS*, for porosity varied between 0 and 1 (Fig. 10). Where rock thermal conductivity is low, e.g. in clay,

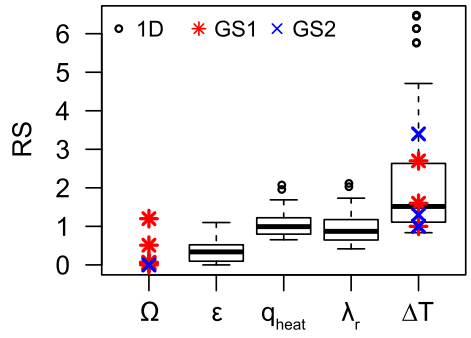

Fig. 10. Relative sensitivity of the maximum permafrost thickness to changes in physical properties and the ΔT-scaling of the surface temperature series. Box-whisker plots represent results from 1D model. Results from the 2D models of GS1 and GS2 are overlain on these for Ω and ΔT.

mudstone or shale lithologies, simulated PF_{max} does not change markedly for a change in porosity.

4.2. Impact of heat advection on permafrost thickness

The inclusion of heat advection in the model was only found to have an effect on the permafrost thickness and distribution where the geological setting has a high hydraulic conductivity and where permafrost is considered to be highly permeable. For the higher hydraulic conductivity setting GS1, heat advection was found to have a minor effect, of up to approximately 10 m, on PF_{max}, when considering permafrost that is six orders less permeable than unfrozen ground ($\Omega = 6$). In contrast, where the hydraulic conductivity of the permafrost decreases by only one order of magnitude ($\Omega = 1$), the effect of heat advection is larger and the influence of advective heat flow on PF_{max} was simulated to be up to approximately 80 m. The effect of advective heat flow is largest when permafrost is shallow, and decreases with increasing permafrost thickness. In the model, where cold water flows vertically downwards beneath hills, heat advection causes thicker permafrost to develop. Where water upwells to topographic lows, heat advection thins permafrost. In contrast, for GS2, the influence of heat advection is simulated to be negligible, since it is a low hydraulic conductivity environment with a low topographic gradient. However, if in GS2 there were hills over the outcropping aquifer similar to the one described in the lowlands of GS1, local impacts of heat advection could be expected. However, this is unlikely to largely impact permafrost thickness at L2.

4.3. Implications for a GDF safety case

The modelling results inform a future assessment of permafrost phenomena for a GDF safety case by providing ranges of maximum permafrost thicknesses, the number of permafrost events, and the maximum duration at which permafrost occurs at a specified depth. Consider the ST_14, and ST_18 simulations, permafrost is modelled as extending to depths of 175 m and 310 m, respectively for GS1, and to 104 m and 160 m, respectively for GS2. In the extreme case (ST_25) this increases to 597 m for GS1 and 320 m for GS2. Permafrost extending to these depths would be accompanied by mechanical effects of freezing and thawing induced by volume change of phase change of water/ice. Direct evidence of permafrost depth in the geological rock record in the UK is very limited/absent (Busby et al., 2016; Murton and Ballantyne, 2017); research to date (Pons-Branchu et al., 2010; Žák et al., 2012; Vaks et al., 2013) focusses on U-series dating of speleothem deposition periods in caves to reconstruct the timing of past periods of permafrost degradation. Elsewhere in Europe, an isolated Cryogenic cave carbonate find indicates that Weichselian permafrost penetrated to a depth of at least 285 m in the High Tatra mountains, Slovakia (Žák et al., 2012). Chemical fingerprinting of permafrost in rock formations, in particular the pore fluids for example, is an area warranting research and would enable an assessment of model performance.

The number of freezing cycles reaching a certain depth may be important in considering the potential changing mechanical properties of a GDF. For example, only for ST_25 simulation of GS1 did permafrost reach a thickness of 400 m (six times), and a thickness of 500 m (four times) over the duration of 1 million years. Shallower depths freeze more often: permafrost thickness exceeded 100 m 19 times at L1 (GS1) and 13 times at L2 (GS2) for ST_25; for ST_14 these event numbers reduce to six and two for L1 and L2, respectively.

The maximum duration of permafrost at a certain depth at a time may be important for considering potential impacts of the freeze-out of solutes and their effect in relation to the possible initiation of convection-driven flow (Vidstrand et al., 2006). The maximum duration permafrost exceeded a thickness of 100 m at L1 (GS1) was simulated to be 70 ka for ST_25 and 20 ka for ST_14. The duration reduces 32 ka when considering a permafrost thickness of 400 m and ST-25 (Table 6). Indirect effects of permafrost on a GDF include changes to the sub-

permafrost hydrogeological system, which we have only discussed briefly in this paper. The existence of permafrost results in a reduction of groundwater recharge, which causes a decrease in sub-permafrost hydraulic heads and a reduction of groundwater flow magnitudes at depth. The freeze over of discharge locations, or the formation of taliks can alter discharge locations and groundwater flow directions (Vidstrand et al., 2014). However, the prediction of the timing of the occurrence and location of these discharge locations would require a land surface evolution model, e.g. as applied in (Hartikainen et al., 2010). In addition, the impacts of permafrost on groundwater flow paths and magnitudes will impact chemical and nuclide transport at depth, and influence their concentration and discharge locations.

4.4. Comparison of simulated permafrost thickness to other UK permafrost estimates

The permafrost thicknesses modelled in this study can be compared to previous modelled permafrost thicknesses at selected locations within the UK. Previously-modelled permafrost thickness in the UK ranges between 30 m and 180 m for the average estimate climate, and between 180 m and 235 m for the cold estimate climate considering the last glacial cycle (Busby et al., 2014). The large range in modelled permafrost thickness is due to different geologies as well as different surface temperature time-series used.

4.5. Modelling assumptions and limitations

To model permafrost thickness, several assumptions regarding the boundary conditions, the stationarity of the system and the simulated processes were made.

The modelling presented in this paper uses generic geological settings and boundary conditions to assess the permafrost thickness. A stationary geological setting is assumed, in which the thermal and hydraulic properties of the geological environment and the topography do not change over time and no erosion or depositions take place. Since we studied generic geological settings, we did not consider the effect of glaciation on the permafrost thickness and the hydrogeology.

4.5.1. Surface temperature time series

The temperature scenarios are applied at the ground surface, and therefore, thermal effects at the ground-atmosphere boundary are not considered separately, but included within the temperature scenario. Whereas there are some reconstructions in minimum temperatures during the LGM in the UK (Coope et al., 1971; Atkinson et al., 1987; Glasser and Siegert, 2002; Annan and Hargreaves, 2013), absolute paleo temperatures further into the past are absent. For the LGM, the range in reconstructed minimum temperatures is large, ranging from −13 °C to −5 °C, or approximately between 24 and 11 °C below present day temperatures, assuming a present mean annual temperature between 6 and 11 °C (Jenkins et al., 2008). In addition to uncertainties associated with estimating the mean annual air temperature, heat exchange occurring in the boundary layer of vegetation, surface organic material and snow alters the ground surface temperature from the surface air temperature by several degrees and varies spatially (Williams and Smith, 1989). Combining the uncertainties in surface air temperature and surface temperature offsets, we scaled the surface temperature time-series between 10 and 25 °C below present day temperatures; the maximum permafrost thickness simulated using the scaled temperature time-series ranges from 51 to 597 m for GS1 and 10 to 320 m for GS2. The Δ*T-25* scenario, which generated the thickest permafrost potentially overestimates the permafrost thickness, since only one proxy record suggests temperatures as low as these (Atkinson et al., 1987). Since other studies (Coope et al., 1971; Glasser and Siegert, 2002; Annan and Hargreaves, 2013; Westaway and Younger, 2013) suggested mean annual temperatures during the Last Glacial Maximum of between −5 °C and − 9 °C, the Δ*T-14* and Δ*T-18* scenarios - which generated simulated permafrost thicknesses of 171–280 m for GS1 and 104–160 m for GS2 - better represents these mean annual temperature estimates. However this can vary locally depending on the magnitude of the surface temperature offset discussed above.

4.5.2. Hydrogeology

In the model, groundwater flow was assumed to be fully saturated and topographically driven, and the effects of salinity on groundwater flow or permafrost formation, as well as cryosuction, ice segregation, or ice wedge formation were not considered. Therefore, the representation of groundwater flow is simplified, which will also affect the representation of heat advection. In addition, to assess the impact of heat advection, there is some uncertainty associated with the relative hydraulic conductivity and the freezing curve of different lithological units. To assess the relative importance of heat advection for a specific GDF location, both the shapes of the freezing curve and the relative hydraulic conductivity function for the respective units would need to be understood. This is especially important for higher hydraulic conductivity units, where heat advection could be significant. Published relative hydraulic conductivity values, derived from laboratory experiments, suggest ranges of variation with ice saturation, or temperature below 0 °C, of six to eight orders of magnitudes lower for sand and three to five orders of magnitudes lower for silt and mud (Burt and Williams, 1976; Kleinberg and Griffin, 2005; Watanabe and Flury, 2008; Azmatch et al., 2012; Kurylyk and Watanabe, 2013). Based on this, within sandstones, the simulations using $\Omega = 6$ are the most likely scenario. However, the relative hydraulic conductivity might decrease at larger spatial scales, as intra-permafrost taliks along fractures or higher permeable zones might persist and increase the overall hydraulic conductivity of the permafrost. Where permafrost is assumed to be relatively permeable ($\Omega = 1$), the modelling here suggests that more permafrost thaw occurs at topographic lows. However, when including a seasonal temperature fluctuation, McKenzie and Voss (2013) suggest that thaw is largest on hilltops where warm water recharges and that thawing occurs more slowly at low-elevation discharge points where water temperatures have cooled to near zero as a result of latent heat loss during thaw.

4.5.3. Glaciation

In this study, we did not considered the effects of glaciation, as the geological settings for this study are generic and not bound to specific locations. We aimed to estimate the maximum impact of permafrost on the geological settings.

Whether glaciation will likely impact a potential GDF location will strongly depend on its geographical location. Some areas within the UK experienced recurrent periglacial conditions with no glaciations during the Quaternary, whereas other regions were glaciated during the Anglian glaciation, or the Anglian and Devensian (Murton and Ballantyne, 2017). The maximum ice extent and the deglaciation history of the last British Ice Sheet is relatively well constrained from glacial geomorphological evidence (Clark et al., 2012; Hughes et al., 2016), and numerical modelling (Boulton and Hagdorn, 2006; Hubbard et al., 2009; Patton et al., 2017), however, the timing of ice coverage during the Quaternary is more uncertain. Evidence for pre-Weichselian Quaternary glaciation in the UK varies geographically; for the NW margin, the North Sea and the southern UK, evidence has been found for the marine isotope stages (MIS) 2, 6, 12. In addition to this, ice coverage potentially occurred during MIS 8 at the NW margin, during MIS 10 at the NW margin and the southern UK, during MIS 18 and 22 in the North Sea and southern UK and potentially MIS 16 and 20 in the Southern UK (Lee et al., 2012). Therefore, there are potential gaps in glaciation during several cold periods, during which extensive permafrost could have formed.

The timing, duration and the temperature of a glacier influences the ground surface temperature. Warm-based, or temperate, ice insulates the ground from the subzero air temperatures, whereas cold-based ice

can potentially be colder than temperatures without ice coverage. Therefore, the impact of glaciation will directly affect the permafrost thickness by altering the ground surface temperature. The temperature difference between surface air temperature and ground surface temperature depends on the geographic location, as this will determine the duration for which a location experiences sub-zero temperatures before an ice sheet will reach there. For example, locations in the Highlands have previously been suggested to be covered by cold based ice during the Devensian (Boulton and Hagdorn, 2006), and would thus have experienced permafrost underneath the ice sheet, but shallower than if it was unglaciated (Busby et al., 2016). In contrast, regions underneath fast-flowing, temperate ice, would only develop permafrost before ice advance or after ice retreat. There, permafrost was estimated to reach 20 m over the past 123 ka (Busby et al., 2016). In contrast, outside the Devensian ice limit, for example in Dartmoor or East Anglia, permafrost would have formed without disturbance from an ice sheet during the Devensian (Busby et al., 2016).

Impacts of glaciation on the hydrogeology at a depth of a GDF are complex and include changes in recharge rates, fracture permeabilities, overburden pressures, and pressures at depth. Recharge into confined aquifers can be much greater than for present day conditions, as confirmed by geochemical data (Grasby and Chen, 2005; Person et al., 2012a; Provost et al., 2012). Glacial meltwater can recharge an aquifer when the glacier bed is wet-based, and can an either originate from in-situ basal melting or from surface melting during the melt season (Zwally et al., 2002; Piotrowski, 2006; Person et al., 2012a). Hydraulic heads underneath warm-based glacier or ice sheet can be near flotation, which is ~90% of the local ice sheet thickness (Piotrowski, 2006; Provost et al., 2012). Glacial erosion and deposition alter the overburden pressure and may affect fluid pressures (Person et al., 2012b). In addition, the weight of an ice sheet results in the deformation of the Earth's surface; direct loading depresses the surface below the ice sheet, resulting in compressive stresses (Lemieux et al., 2008b; Neuzil, 2012). Mechanical loading differs from hydrological driven changes as changes in boundary stress propagate almost instantaneously through the subsurface, the stress changes alter fluid pressures primarily in the least permeable units, and mechanical loading can alter how permeability is structured (Neuzil, 2012). In addition, bending of the lithosphere under the ice weight, results in horizontal tensile stresses, or flexural loading (Lemieux et al., 2008b; Neuzil, 2012). Flexural loading may result in stress-mediated changes in fracture permeability (Neuzil, 2012). Laboratory experiments have shown that permeability decreased by two orders of magnitude applying direct loading equivalent of a 2 km thick ice sheet. In contrast, altering the stress ratio to represent conditions of a retreating 2 km thick ice sheet before flexural stresses have relaxed, an increase in horizontal permeability of nearly an order of magnitude and a decrease in vertical permeability of a factor of four were observed (Min et al., 2004; Neuzil, 2012). The existence of brines in deeper parts of the aquifer and flushing of cold and fresh, glacially recharged groundwater results in large density differences in the waters, and therefore, fluid flow is also driven by buoyancy forces caused by variations in solute concentration, temperature and pressure (Lemieux et al., 2008b; Provost et al., 2012). If perennially frozen ground underlies the glacial forefield, glacially recharged groundwater is forced under the permafrost (Person et al., 2012b). Groundwater then discharges either near the ice sheet margin by hydrofracturing the sediments (Boulton et al., 1993), into taliks under surface water bodies (Scheidegger and Bense, 2014) or at the sea (Boulton et al., 1993). These zones might be of special importance for a GDF safety assessment.

For any hydrogeological and permafrost assessment over glacial-interglacial time-scales at a specific location which is likely to be glaciated, a glacial model is required that provides ice sheet thickness, extent, subglacial temperature and water fluxes, and isostatic response. These can be used as boundary conditions for hydrogeological and permafrost models to assess the impact of glaciation on permafrost thickness and the hydrogeological system. In addition, if the geological environment is saline, or salinity increases with depth, effects of salinity on freeze-thaw, as well as any indirect effects of changes in salinity due to freeze out of solutes or recharge of fresh glacial meltwater, will need to be considered. Since coupling a permafrost, groundwater and glacial model is numerically challenging, both permafrost and glacial processes could be provided as boundary conditions into a groundwater model, as for example was done for the Canadian Shield (Lemieux et al., 2008c).

5. Conclusions

In this study, we used numerical modelling of coupled heat and fluid flow to evaluate the sensitivity of simulated maximum permafrost thickness and dynamics to a variety of climatic scenarios, and subsurface thermo-hydrogeological properties, and how permafrost permeability-influenced heat advection affects permafrost development for two geological settings: sandstones overlying HSR (GS1) and a mixed sedimentary sequence overlying HSR (GS2). In addition, we conducted a sensitivity analysis, estimating the sensitivity of maximum permafrost thickness to model parameter values, considering plausible ranges of physical properties for potential GDF host rocks in the UK.

The modelling has shown that maximum permafrost thickness is most sensitive to the surface temperature boundary condition applied, and that the uncertainty associated with this must be considered carefully if a site-specific assessment is to be made as part of a GDF safety case. Maximum permafrost thicknesses simulated using scaled surface temperatures of 10, 14, 18 and 25 °C below present day, were: 51 m, 175 m, 310 m, and 597 m for L1 (GS1), respectively; and 10 m, 104 m, 160 m, and 320 m for L2 (GS2), respectively.

The study of the sensitivity of maximum permafrost thickness to thermo-hydrogeological property parameters, based on available data for UK lithological units, has shown that PF_{max} depends on thermal conductivity, latent heat and geothermal heat flow. The relative importance of each of these factors, however, depends on the magnitude of the other factors. Greater permafrost thickness is to be expected where there is a low geothermal heat flux, a high thermal conductivity and a low porosity. The relative sensitivity of PF_{max} to geothermal heat flux and thermal conductivity are comparable and approximately double that of porosity. PF_{max} is most sensitive to: a change in thermal conductivity where porosity and geothermal heat flux are low; to a change in geothermal heat flux, where thermal conductivity is high and porosity is low; and to a change in porosity where thermal conductivity is high and geothermal heat flux is low.

When considering the maximum permafrost thickness at potential GDF location, we suggest fully exploring the uncertainty of the surface temperature time-series, to derive bounds of potential permafrost thicknesses. The maximum permafrost thickness can vary considerably depending on thermo-hydrogeological properties, as shown for the two settings presented here with the relative importance of the different thermal properties being non-linear and dependent on the magnitude of the other properties. Local differences in permafrost thickness caused by heat advection are of minor importance over the timeframe of glacial cycles, however heat advection can be important in the development of taliks and the associated maintenance of a more active groundwater flow system, and therefore it is important to represent these processes when considering effects of permafrost on the groundwater flow system within more permeable lithological sequences.

Acknowledgements

This research was funded by Radioactive Waste Management Limited, with some additional support from core science funding of the British Geological Survey. We would like to thank Jon Busby at the British Geological Survey for his advice about the research. Authors Scheidegger, McEvoy and Jackson publish with the permission of the Executive Director of the British Geological Survey.

Appendix A

A.1. Heat transport

The subsurface temperature distributions (T [K]) are calculated using the advection-diffusion equation, including the transient effects of latent heat of fusion (L_f [J m^{-3}]) to simulate freezing and thawing as follows:

$$\nabla \cdot [\lambda_e \nabla T] - C_w \vec{q} \cdot \nabla T = C_p \frac{\partial T}{\partial t} + L_f \frac{\partial \Theta_w}{\partial t} \tag{A.1}$$

where λ_e [W m^{-1} K^{-1}] is the effective thermal conductivity the rock/water/ice mixture, C_w [J m^{-3} K^{-1}] is the heat capacity of water, C_p [J m^{-3} K^{-1}] is the effective heat capacity of the rock/water/ice composite, $\vec{q}$ [m s^{-1}] is the Darcy flux and is coupled with the fluid flow equation.

For a fully saturated media, all free pore space is filled with water/ice: $\theta_r + \theta_w + \theta_i = 1$, where $\theta_w = \varepsilon S_w$ and $\theta_i = \varepsilon - \theta_w$. The porosity is ε [−], and the volume fractions of solid, water and ice are θ_r, θ_w, θ_i respectively. It is assumed that porosity remains constant over time, and hence no soil consolidation, frost heave or thaw settlement is considered (Bear and Bachmat, 2012). The water saturation curve S_w is described with a smoothed Heaviside function, which is a built in step-function in COMSOL Multiphysics (COMSOL, 2016). The function is dependent on T [°C], the freezing interval d [°C], and the residual saturation, S_{wres}:

$$\begin{gathered} S_{wres}, \text{if } T \le -d \\ 1, \text{if } T \ge 0 \\ 0.5 + \frac{S_{wres}}{2} + (1 - S_{wres})\left(0.9375\left(\frac{T+d}{d}\right) - 0.625\left(\frac{T+d}{d}\right)^3 \right. \\ \left. + 0.1875\left(\frac{T+d}{d}\right)^5\right), \text{if } 0 < T > S_{wres} \end{gathered} \tag{A.2}$$

The Heaviside function compares closely to the error function as described in Bense et al. (2009) which has previously been used as a soil freezing function (Bense et al., 2009; Bense et al., 2012; Scheidegger and Bense, 2014).

The thermal conductivity of ice is more than four times higher than that of water, and thus frozen ground has a higher thermal conductivity than unfrozen ground (Williams and Smith, 1989; Woo, 2012). The effective thermal conductivity of rock λ_e [W m^{-1} K^{-1}] is calculated as a weighted geometric mean from the thermal conductivities of rock (λ_r), water (λ_w) and ice (λ_i): $\lambda_e = \lambda_r^{\Theta_r} \lambda_w^{\Theta_w} \lambda_i^{\Theta_i}$. In this paper, thermal conductivity is assumed to be isotropic.

Thermal equilibrium between the solid, liquid and ice phase is assumed and for a composite material, a weighted average for the mass heat capacities [J kg^{-1} K^{-1}] of rock matrix (C_r), water (C_w) and ice (C_i) multiplied by their density (ρ [kg m^{-3}]) is used: $C_e = C_r \Theta_r \rho_r + C_w \Theta_w \rho_w + C_i \Theta_i \rho_i$. The volumetric heat capacity C_e [J m^{-3} K^{-1}] is the amount of heat required to change the temperature of 1 m^3 by 1 °C.

A.2. Fluid transport

Fluid flow is simulated using fully saturated fluid flow described by Darcy's Law, and using the assumption that the solid matrix is immobile. The transient hydraulic head (h [m]) field is calculated as follows:

$$-\nabla \cdot [k_{rw} K \nabla h] = S_w S_s \frac{\partial h}{\partial t} + \varepsilon \frac{(\rho_i - \rho_w)}{\rho_w} \frac{\partial S_w}{\partial t} \tag{B.1}$$

where K [m s^{-1}] is the hydraulic conductivity, k_{rw} [−], is the relative hydraulic conductivity as a function of water saturation, S_w [−] is the water saturation, ρ_w [kg m^{-3}] and ρ_i [kg m^{-3}] the density of water and ice, S_s [m^{-1}] the aquifer specific storage, and ε the porosity. For fully saturated media, $S_w = 1 - S_i$. Subscripts of w and i refer to liquid water and ice. The term $\varepsilon \frac{(\rho_i - \rho_w)}{\rho_w} \frac{\partial S_w}{\partial t}$ describes a source/sink term that is related to the volume change between water and ice. When ice forms, the volume of the water fraction expands and the hydraulic head increases. When ice melts, the volume of water drops and generates a drop in hydraulic head. It is assumed in the model that the density and viscosity of water are constant.

A.2.1. Relative hydraulic conductivity

In perennially frozen ground, ice clogs the open pore space and restricts water flow (McKenzie et al., 2007). However, over the freezing process, porewater freezes progressively from larger pores through to smaller pores and there will be a steep decrease in hydraulic conductivity (Ireson et al., 2013). How groundwater flow decreases over the freezing interval has a profound control on how permafrost and changes in permafrost distribution impacts groundwater flow. The decrease in hydraulic conductivity over the freezing interval can be represented with a relative hydraulic conductivity curve (k_{rw}) (McKenzie et al., 2007). Here, a similar approach to Hansson et al. (2004) is taken:

$$k_{rw} = 10^{-(1 - S_w)\Omega} \tag{B.2}$$

where $\Omega = 6$. This means that the relative hydraulic conductivity decreases six orders of magnitude.

References

Annan, J.D., Hargreaves, J.C., 2013. A new global reconstruction of temperature changes at the Last Glacial Maximum. Clim. Past 9, 367–376.

Atkinson, T.C., Briffa, K.R., Coope, G.R., 1987. Seasonal temperatures in Britain during the past 22,000 years, reconstructed using beetle remains. Nature 325, 587–592.

Azmatch, T.F., Sego, D.C., Arenson, L.U., Biggar, K.W., 2012. Using soil freezing characteristic curve to estimate the hydraulic conductivity function of partially frozen soils. Cold Reg. Sci. Technol. 83–84, 103–109.

Bear, J., Bachmat, Y., 2012. Introduction to Modeling of Transport Phenomena in Porous Media. vol. 4. Springer Science & Business Media.

Bense, V.F., Person, M.A., 2008. Transient hydrodynamics within intercratonic sedimentary basins during glacial cycles. J. Geophys. Res. Earth Surf. 113.

Bense, V.F., Ferguson, G., Kooi, H., 2009. Evolution of shallow groundwater flow systems in areas of degrading permafrost. Geophys. Res. Lett. 36.

Bense, V.F., Kooi, H., Ferguson, G., Read, T., 2012. Permafrost degradation as a control on hydrogeological regime shifts in a warming climate. J. Geophys. Res. Earth Surf. 117.

Bintanja, R., van de Wal, R.S.W., Oerlemans, J., 2005. Modelled atmospheric temperatures and global sea levels over the past million years. Nature 437, 125.

Boulton, G.S., Hagdorn, M., 2006. Glaciology of the British Isles Ice Sheet during the last glacial cycle: form, flow, streams and lobes. Quat. Sci. Rev. 25, 3359–3390.

Boulton, G.S., Slot, T., Blessing, K., Glasbergen, P., Leijnse, T., Vangijssel, K., 1993. Deep circulation of groundwater in overpressured subglacial aquifers and its geological consequences. Quat. Sci. Rev. 12, 739–745.

Burley, A.J., Edmunds, W.M., 1978. Catalogue of Geothermal Data for the Land Area of the United Kingdom.

Burley, A., Gale, I., 1982. Catalogue of Geothermal Data for the Land Area of the United Kingdom, First Revision August 1981. Investigation of the Geothermal Potential of the UK. p. 4.

Burley, A.J., Edmunds, W.M., Gale, I.N., 1984. Investigation of the Geothermal Potential of the UK: Catalogue of Geothermal Data for the Land Area of the United Kingdom. British Geological Survey.

Burt, T.P., Williams, P.J., 1976. Hydraulic conducitivity in frozen soils. Earth Surf. Process. Landf. 1, 349–360.

Busby, J.P., Terrington, R., 2017. Assessment of the resource base for engineered geothermal systems in Great Britain. Geotherm. Energy 5.

Busby, J.P., Kingdon, A., Williams, J., 2011. The measured shallow temperature field in Britain. Q. J. Eng. Geol. Hydrogeol. 44, 373–387.

Busby, J.P., Kender, S., Williamson, J.P., Lee, J.R., 2014. Regional Modelling of the Potential for Permafrost Development in Great Britain.

Busby, J.P., Lee, J.R., Kender, S., Williamson, J.P., Norris, S., 2015. Modelling the potential for permafrost development on a radioactive wate geological disposal facility in Great Britain. Proc. Geol. Assoc. 126, 664–674.

Busby, J.P., Lee, J.R., Kender, S., Williamson, P., Norris, S., 2016. Regional modelling of permafrost thicknesses over the past 130 ka: implications for permafrost development in Great Britain. Boreas 45, 46–60.

Candy, B.S., Lee, J., 2011. Climates of the early Middle Pleistocene in Britain: environments of the earliest humans in northern Europe. In: Candy, B.S., Lee, J. (Eds.), The Ancient Human Occupation of Britain. Elsevier Science Publishers B.V., North-Holland, pp. 11–22.

Chan, T., Stanchell, F.W., 2009. Implications of subsurface thermal-hydraulic-mechanical processes associated with glaciation on Shield flow system evolution and performance assessment. Environ. Geol. 57, 1371–1389.

Clark, C.D., Hughes, A.L.C., Greenwood, S.L., Jordan, C., Sejrup, H.P., 2012. Pattern and timing of retreat of the last British-Ice Sheet. Quat. Sci. Rev. 44, 112–146.

COMSOL, 2016. COMSOL Multiphysics. http://www.comsol.com/.

Coope, G.R., Morgan, A., Osborne, P.J., 1971. Fossil Coleoptera as indicators of climatic fluctuations during the last glaciation in Britain. Palaeogeogr. Palaeoclimatol. Palaeoecol. 87–101.
DECC, 2014. Implementing Geological Disposal: A Framework for the Long-term Management of Higher Activity Radioactive Waste UK Government Policy Paper. Department of Energy & Climate Change https://www.gov.uk/government/publications/implementing-geological-disposal.
Downing, R.A., Gray, D.A., 1986. Geothermal resources of the United Kingdom. J. Geol. Soc. 143, 499–507.
Fischer, U.H., Bebiolka, A., Brandefelt, J., Follin, S., Hirschorn, S., Jensen, M., et al., 2015. Chapter 11 - radioactive waste under conditions of future ice ages. In: Fischer, U.H., Bebiolka, A., Brandefelt, J., Follin, S., Hirschorn, S., Jensen, M., et al. (Eds.), Snow and Ice-related Hazards, Risks and Disasters. Academic Press, Boston, pp. 345–393.
Ge, S., McKenzie, J., Voss, C., Wu, Q., 2011. Exchange of groundwater and surface-water mediated by permafrost response to seasonal and long term air temperature variation. Geophys. Res. Lett. 38, L14402.
Glasser, N.F., Siegert, M.J., 2002. Calculating basal temperatures in ice sheets: an excel spreadsheet method. Earth Surf. Process. Landf. 27, 673–680.
Grasby, S.E., Chen, Z.H., 2005. Subglacial recharge into the Western Canada Sedimentary Basin - impact of pleistocene glaciation on basin hydrodynamics. Geol. Soc. Am. Bull. 117, 500–514.
Grenier, C., Régnier, D., Mouche, E., Benabderrahmane, H., Costard, F., Davy, P., 2013. Impact of permafrost development on groundwater flow patterns: a numerical study considering freezing cycles on a two-dimensional vertical cut through a generic river-plain system. Hydrogeol. J. 21, 257–270.
Grenier, C., Anbergen, H., Bense, V., Chanzy, Q., Coon, E., Collier, N., et al., 2018. Groundwater flow and heat transport for systems undergoing freeze-thaw: Intercomparison of numerical simulators for 2D test cases. Adv. Water Resour. 114, 196–218.
Hansson, K., Simunek, J., Mizoguchi, M., Lundin, L.C., van Genuchten, M.T., 2004. Water flow and heat transport in frozen soil: numerical solution and freeze-thaw applications. Vadose Zone J. 3, 593–704.
Hartikainen, J., Kouhia, R., Wallroth, T., 2010. Permafrost Simulations at Forsmark Using a Numerical 2D Thermo-hydro-chemical Model.
Holmén, J., Benabderrahmane, H., Buoro, A., Brulhet, J., 2011. Modelling of permafrost freezing and melting and the impact of a climatic cycle on groundwater flow at the Meuse/Haute-Marne site. Phys. Chem. Earth Parts A/B/C 36, 1531–1538.
Hubbard, A., Bradwell, T., Golledge, N., Hall, A., Patton, H., Sugden, D., et al., 2009. Dynamic cycles, ice streams and their impact on the extent, chronology and deglaciation of the British–Irish ice sheet. Quat. Sci. Rev. 28, 758–776.
Hughes, A.L.C., Gyllencreutz, R., Lohne, Ø.S., Mangerud, J., Svendsen, J.I., 2016. The last Eurasian ice sheets – a chronological database and time-slice reconstruction, DATED-1. Boreas 45, 1–45.
IAEA, 2011. Geological disposal facilities for radioactive waste: specific safety guide. No. SSG-14. https://www-pub.iaea.org/books/IAEABooks/8535/Geological-Disposal-Facilities-for-Radioactive-Waste.
Ireson, A., van der Kamp, G., Ferguson, G., Wheater, H., 2013. Hydrogeological processes in seasonally frozen northern latitudes: understanding gaps and challenges. Hydrogeol. J. 21, 53–66.
Jenkins, G.J., Perry, M.C., Prior, M.J., 2008. The Climate of the United Kingdom and Recent Trends. Met Office Hadley Centre, Exeter, UK.
Kleinberg, R.L., Griffin, D.D., 2005. NMR measurements of permafrost: unfrozen water assay, pore-scale distribution of ice, and hydraulic permeability of sediments. Cold Reg. Sci. Technol. 42, 63–77.
Kurylyk, B.L., Watanabe, K., 2013. The mathematical representation of freezing and thawing processes in variably-saturated, non-deformable soils. Adv. Water Resour. 60, 160–177.
Lee, J.R., Busschers, F.S., Sejrup, H.P., 2012. Pre-Weichselian Quaternary glaciations of the British Isles, The Netherlands, Norway and adjacent marine areas south of 68°N: implications for a long-term ice sheet development in northern Europe. Quat. Sci. Rev. 44, 213–228.
Lemieux, J.M., Sudicky, E.A., Peltier, W.R., Tarasov, L., 2008a. Dynamics of groundwater recharge and seepage over the Canadian landscape during the Wisconsinian glaciation. J. Geophys. Res. Earth Surf. 113.
Lemieux, J.M., Sudicky, E.A., Peltier, W.R., Tarasov, L., 2008b. Simulating the impact of glaciations on continental groundwater flow systems: 1. Relevant processes and model formulation. J. Geophys. Res. Earth Surf. 113.
Lemieux, J.M., Sudicky, E.A., Peltier, W.R., Tarasov, L., 2008c. Simulating the impact of glaciations on continental groundwater flow systems: 2. Model application to the Wisconsinian glaciation over the Canadian landscape. J. Geophys. Res. Earth Surf. 113.
Lisiecki, L.E., Raymo, M.E., 2005. A Pliocene-Pleistocene stack of 57 globally distributed benthic δ18O records. Paleoceanography 20.
McEvoy, F.M., Schofield, D.I., Shaw, R.P., Norris, S., 2016. Tectonic and climatic considerations for deep geological disposal of radioactive waste: a UK perspective. Sci. Total Environ. 571, 507–521.
McEwen, T., de Marsily, G., 1991. The Potential Significance of Permafrost to the Behaviour of a Deep Radiactive Waste Repository.
McKenzie, J.M., Voss, C.I., 2013. Permafrost thaw in a nested groundwater-flow system. Hydrogeol. J. 21, 299–316.
McKenzie, J.M., Voss, C.I., Siegel, D.I., 2007. Groundwater flow with energy transport and water-ice phase change: numerical simulations, benchmarks, and application to freezing in peat bogs. Adv. Water Resour. 30, 966–983.
McKeown, C., Haszeldine, R.S., Couples, G.D., 1999. Mathematical modelling of groundwater flow at Sellafield, UK. Eng. Geol. 52, 231–250.
Min, K., Rutqvist, J., Tsang, C., Jing, L., 2004. Stress-dependent permeability of fractured rock masses: a numerical study. Int. J. Rock Mech. Min. Sci. 41, 1191–1210.
Murton, J.B., Ballantyne, C.K., 2017. Periglacial and permafrost ground models for Great Britain. In: Murton, J.B., Ballantyne, C.K. (Eds.), Engineering Geology and Geomorphology of Glaciated and Periglaciated Terrains. The Geological Society, London.
Nasir, O., Fall, M., Nguyen, S.T., Evgin, E., 2013. Modeling of the thermo-hydro-mechanical-chemical response of sedimentary rocks to past glaciations. Int. J. Rock Mech. Min. Sci. 64, 160–174.
Näslund, J.O., Brandefelt, J., 2014. Timing of future glacial inception. In: Näslund, J.O., Brandefelt, J. (Eds.), Snow and Ice-related Hazards, Risks and Disasters. Elsevier, Oxford.
NDA, 2010. Geological disposal: generic post-closure safety assessment. NDA report no. NDA/RWMD/030. https://rwm.nda.gov.uk/publication/geological-disposal-generic-post-closure-safety-assessment/.
Neuzil, C.E., 2012. Hydromechanical effects of continental glaciation on groundwater systems. Geofluids 12, 22–37.
Normani, S.D., Sykes, J.F., 2012. Paleohydrogeologic simulations of Laurentide ice-sheet history on groundwater at the eastern flank of the Michigan Basin. Geofluids 12, 97–122.
Patton, H., Hubbard, A., Andreassen, K., Auriac, A., Whitehouse, P.L., Stroeven, A.P., et al., 2017. Deglaciation of the Eurasian ice sheet complex. Quat. Sci. Rev. 169, 148–172.
Person, M., Bense, V., Cohen, D., Banerjee, A., 2012a. Models of ice-sheet hydrogeologic interactions: a review. Geofluids 12, 58–78.
Person, M., Mcintosh, J., Iverson, N., Neuzil, C.E., Bense, V., 2012b. Geologic isolation of nuclear waste at high latitudes: the role of ice sheets. Geofluids 12, 1–6.
Piotrowski, J.A., 2006. Groundwater under ice sheets and glaciers. In: Piotrowski, J.A. (Ed.), Glacier Science and Environmental Change. Blackwell Publishing, Oxford, pp. 50–59.
Pons-Branchu, E., Hamelin, B., Losson, B., Jaillet, S., Brulhet, J., 2010. Speleothem evidence of warm episodes in northeast France during Marine Oxygen Isotope Stage 3 and implications for permafrost distribution in northern Europe. Quat. Res. 74, 246–251.
Posiva, O., 2012. Safety case for the disposal of spent nuclear fuel at Olkiluoto–synthesis 2012. POSIVA 2012-12. http://www.posiva.fi/files/2987/Posiva_2012-12web.pdf.
Provost, A.M., Voss, C.I., Neuzil, C.E., 2012. Glaciation and regional groundwater flow in the Fennoscandian shield. Geofluids 12, 79–96.
Rollin, K.E., 1987. The geothermal environment in Scotland. Mod. Geol. 11, 235–250.
Rollin, K.E., 1995. A simple heat-flow quality function and appraisal of heat-flow measurements and heat-flow estimates from the UK Geothermal Catalogue. Tectonophysics 244, 185–196.
Rose, J., 2009. Early and Middle Pleistocene landscapes of eastern England. Proc. Geol. Assoc. 120, 3–33.
Ruskeemiemi, T., Paananen, M., Ahonen, L., Kaija, J., Kuivamäki, A., Frape, S., et al., 2002. Permafrost at Lupin. Report of Phase I. Geological Survey of Finland, Nuclear Waste Disposal Research, Permafrost Project GTK-SKB-POSIVA-NIREX-OPG.
RWM, 2016. Geological Disposal. Geosphere Status Report. https://rwm.nda.gov.uk/publication/geological-disposal-geosphere-status-report-december-2010/?download.
Scheidegger, J.M., Bense, V.F., 2014. Impacts of glacially recharged groundwater flow systems on talik evolution. J. Geophys. Res. Earth Surf. 119, 758–778.
Scheidegger, J., Busby, J.P., Jackson, C., McEvoy, F.M., Shaw, R.P., 2017. Coupled modelling of permafrost and groundwater. A case study approach. http://nora.nerc.ac.uk/id/eprint/519040/.
SKB, 2011. Long-term Safety for the Final Repository for Spent Nuclear Fuel at Forsmark. Main Report on the SR-Site Project. SKB TR-11-01. Svensk Kärnbränslehantering AB http://skb.se/upload/publications/pdf/TR-11-01_vol1.pdf.
SKB, 2014. Climate and Climate-related Issues for the Safety Assessment SR-PSU. SKB TR-13-05. Svensk Kärnbränslehantering AB http://skb.se/upload/publications/pdf/TR-13-05.pdf.
Sterckx, A., Lemieux, J.-M., Vaikmäe, R., 2018. Assessment of paleo-recharge under the Fennoscandian Ice Sheet and its impact on regional groundwater flow in the northern Baltic Artesian Basin using a numerical model. Hydrogeol. J. 26, 1–18.
Towler, G.H., Barker, J.A., McGarry, R.G., Watson, S.P., McEwen, T., Michie, U., et al., 2008. Post-closure Perfomrance Assessment: Example Approaches for Groundwater Modelling of Generic Environments. https://rwm.nda.gov.uk/publication/post-closure-performance-assessment-example-approaches-for-groundwater-modelling-of-generic-environments-qrs1378g-1/?download.
Vaks, A., Gutareva, O.S., Breitenbach, S.F.M., Avirmed, E., Mason, A.J., Thomas, A.L., et al., 2013. Speleothems reveal 500,000-year history of Siberian permafrost. Science 340, 183–186.
Vidstrand, P., Svensson, U., Follin, S., 2006. Simulation of Hydrodynamic Effects of Salt Rejection Due to Permafrost. Hydrogeological Numerical Model of Density-driven Mixing, at a Regional Scale, Due to a High Salinity Pulse.
Vidstrand, P., Follin, S., Selroos, J.O., Naslund, J.O., 2014. Groundwater flow modeling of periods with periglacial and glacial climate conditions for the safety assessment of the proposed high-level nuclear waste repository site at Forsmark, Sweden. Hydrogeol. J. 22, 1251–1267.
Watanabe, K., Flury, M., 2008. Capillary bundle model of hydraulic conductivity for frozen soil. Water Resour. Res. 44.
Westaway, R., Younger, P.L., 2013. Accounting for palaeoclimate and topography: a rigorous approach to correction of the British geothermal dataset. Geothermics 48, 31–51.
Williams, P., Smith, M., 1989. The Frozen Earth, Fundamental of Geocryology. Cambridge University Press.
Woo, M.-K., 2012. Permafrost Hydrogeology. Springer, Heidelberg.
Žák, K., Richter, D.K., Filippi, M., Živor, R., Deininger, M., Mangini, A., et al., 2012. Coarsely crystalline cryogenic cave carbonate – a new archive to estimate the Last Glacial minimum permafrost depth in Central Europe. Clim. Past 8, 1821–1837.
Zwally, H.J., Abdalati, W., Herring, T., Larson, K., Saba, J., Steffen, K., 2002. Surface melt-induced acceleration of Greenland ice-sheet flow. Science 297, 218–222.